$$C_2(\text{Gas}) = \frac{C_0(\text{Gas}) - C_1(\text{GasTotal}) \cdot \left(\frac{C_0(\text{heme})}{C_1(\text{heme})}\right)}{\left(1 - \frac{C_0(\text{heme})}{C_1(\text{heme})}\right)} \quad \text{(Eq. 9)}$$

where the following variables are used. C_0(Gas) is the initial gas concentration; C_2(Gas) is at the boundary condition (in the bulk solution); C_1(GasTotal) is the sum of the bound and unbound gas molecules in HbV; C_o(heme) is the total heme concentration in the solution (1.5 μM); and C_1(heme) is the heme concentration in HbV (such as 21,700 μM at $[Hb]_{in}$ = 35 g/dl).

The level of unbound free heme, R, can be expressed as Equation 10, which is used to calculate the levels of reactions for 100 ms and the apparent rate constants from the initial slopes (5 ms).

$$R = \frac{\sum_j V_j \cdot C_{\text{heme}}(t_i, x_j)}{\sum_j V_j \cdot C_{\text{heme}}(t_0, x_j)} \quad \text{(Eq. 10)}$$

RESULTS

NO Binding and CO Binding Profiles of HbV Using Stopped-flow Spectrophotometry—The complete deoxygenation of HbV was clearly confirmed according to the characteristic wavelength of the maximum absorption (λ_{max}) at 430 nm. Because of the strong light-scattering effect of the HbV suspension in comparison with Hb solution and RBC (49), the absorption peaks in the Q band region were not clear in this measurement. After rapid mixing with NO, the immediate absorbance reduction at 430 nm and the increase at 418 nm that correspond to the formation of nitrosylhemoglobin were confirmed (Fig. 1). In the case of mixing with CO, the immediate absorption increase at 419 nm was confirmed. The change of absorption at 430 nm in both reactions was single exponential and indicative of the formation of nitrosylhemoglobin or carbonylhemoglobin in the vesicles.

Time Courses of NO Binding and CO Binding to HbV with Various $[Hb]_{in}$—The scans of spectrophotometry in Fig. 1 were performed three times, and the average level of reaction was plotted as a ratio of absorbance at 430 nm (ΔA_t) at time t, to the initial absorbance (ΔA_0) at time 0 (Fig. 2). The *graph* shows that the NO binding is retarded with increasing $[Hb]_{in}$ from 1 to 35 g/dl. However, no such change was observed in the case of CO binding. From the slopes shown in Fig. 2, the apparent binding rate constants of $k'_{on}{}^{(NO)}$ for NO and $k'_{on}{}^{(CO)}$ for CO were obtained according to Equation 1 and were plotted against $[Hb]_{in}$ (Fig. 3*A*). This clearly shows that $k'_{on}{}^{(NO)}$ is dependent on $[Hb]_{in}$; it decreases from 2.6×10^7 to 0.9×10^7 M^{-1} s^{-1} with increasing $[Hb]_{in}$ from 1 to 35 g/dl. It must be emphasized that $k'_{on}{}^{(NO)}$ at $[Hb]_{in}$ = 1 g/dl was almost identical to $k_{on}{}^{(NO)}$ of a cell-free Hb solution (2.7×10^7 M^{-1} s^{-1}). On the other hand, $k'_{on}{}^{(CO)}$ values at $[Hb]_{in}$ = 1 and 35 g/dl were 3.1×10^5 and 3.0×10^5 M^{-1} s^{-1}, respectively, and almost identical at any $[Hb]_{in}$ and even to $k_{on}{}^{(CO)}$ of a cell-free Hb solution.

Time Courses of NO Binding and CO Binding to HbV with Different Particle Sizes—The influence of particle size was investigated. At the same $[Hb]_{in}$ (35 g/dl), HbVs with different particle sizes were prepared. As shown in Fig. 3*B*, $k'_{on}{}^{(NO)}$ decreased from 1.5×10^7 M^{-1} s^{-1} to 6.5×10^6 M^{-1} s^{-1} with increasing the diameter from 178 ± 74 to 452 ± 184 nm. On the other hand, CO binding showed no such remarkable changes.

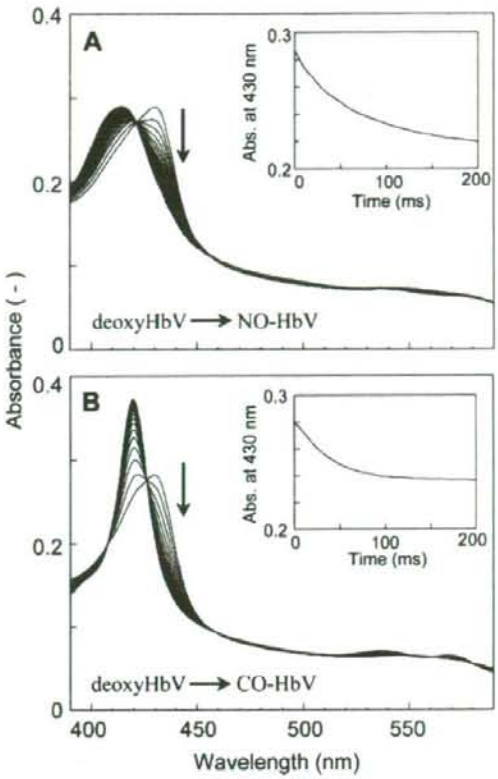

FIGURE 1. **Representative profiles of the reactions of NO or CO with deoxygenated HbV ($[Hb]_{in}$ = 35 g/dl) using stopped-flow spectrophotometry.** *A*, a NO-bubbled PBS ([NO] = 3.8 μM) and HbV in PBS ([heme] = 3.0 μM) were mixed rapidly using a stopped-flow spectrophotometer; the absorption spectra were collected every millisecond over 0.2 s after mixing. In this figure, the spectroscopic curves of every 10 ms are selected. This *panel* shows clearly that the spectrum of deoxyHbV is mostly converted to NO-HbV in 0.2 s. *Inset*, the time course of the measured absorbance at 430 nm. *B*, a CO-bubbled PBS ([CO] = 135 μM) and HbV in PBS ([heme] = 3.0 μM) were mixed rapidly using a stopped-flow spectrophotometer; the absorption spectra were collected every millisecond over 0.2 s after mixing. In this *panel*, the spectroscopic curves of every 10 ms were selected. This *panel* clearly shows that the spectrum of deoxyHbV is mostly converted to CO-HbV in 0.2 s. *Inset*, the time course of the measured absorbance at 430 nm. The optical path length was 1 cm. All of the experiments were performed at 25 °C.

Computer Simulations of NO Binding and CO Binding to HbV—Computer simulations of the experimental results of NO and CO bindings to HbV at different $[Hb]_{in}$ (1–35 g/dl) and different particle diameters (50, 100, 200, 250, and 500 nm) were performed, and the obtained $k'_{on}{}^{(NO)}$ and $k'_{on}{}^{(CO)}$ were plotted on Fig. 3. It was clearly recreated that the NO binding is influenced significantly by $[Hb]_{in}$ and the particle size. Although there were deviations from the experimental results, the NO binding was retarded with increasing $[Hb]_{in}$ from 1 to 35 g/dl. On the other hand, no such change existed in the case of CO binding, and the simulations fit well with the experimental results (Fig. 3*A*). The

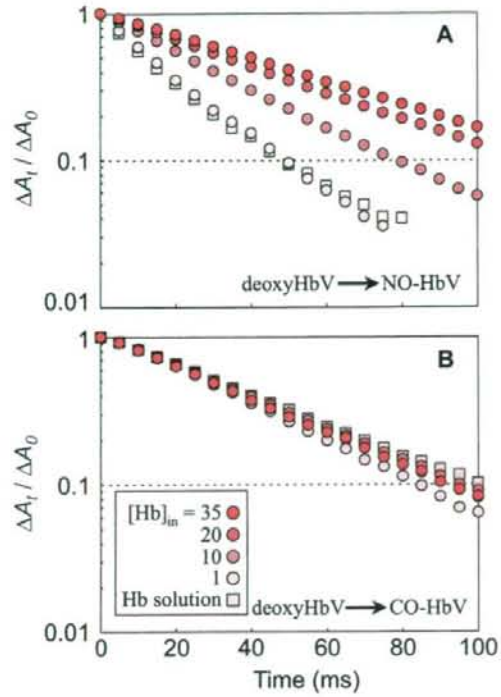

FIGURE 2. **Time courses of NO binding and CO binding by deoxygenated HbV with various $[Hb]_{in}$.** A NO-bubbled PBS (3.8 μM) (*A*) or a CO-bubbled PBS (135 μM) (*B*) and HbVs in PBS ([heme] = 3.0 μM) were mixed rapidly using a stopped-flow spectrophotometer. $[Hb]_{in}$ varies from 1 to 35 g/dl ([heme] = 620–21700 μM); thus, the number of particles differs at the constant [heme] (3.0 μM) in each solution. The level of reaction was plotted on a semilogarithmic *graph* as a ratio of absorption at 430 nm (ΔA_t) at time *t*, to the initial absorption (ΔA_0) at time 0. The results of the cell-free Hb solutions are also plotted, which are almost identical with those of HbV at $[Hb]_{in}$ = 1 g/dl. The *graph* shows that the NO binding rate is retarded with increasing $[Hb]_{in}$ in *A*. However, such a change was not apparent in the case of CO binding in *B*. All of the experiments were performed at 25 °C.

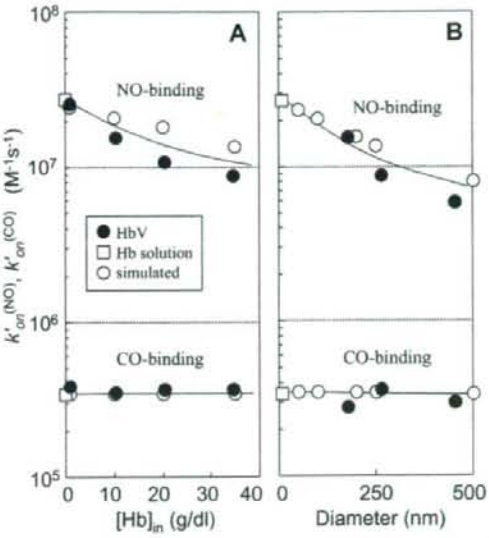

FIGURE 3. **Apparent binding rate constants of NO ($k'_{on}{}^{(NO)}$) and CO ($k'_{on}{}^{(CO)}$) of experimental results and computer simulations.** *A*, plotted against $[Hb]_{in}$ of HbV; *B*, plotted against particle diameter. *A*, the apparent binding rate constants (experimental) were calculated from the slopes in Fig. 2. Values of the exact $k_{on}{}^{(NO)}$ and $k_{on}{}^{(CO)}$ of the elementary reactions of cell-free Hb solution are also plotted on the *vertical axis*. Those of computer simulations (diameter, 250 nm) are plotted as *open circles*. *B*, the apparent binding rate constants were calculated similarly and plotted against the particle diameter. Values of the exact $k_{on}{}^{(NO)}$ and $k_{on}{}^{(CO)}$ of cell-free Hb solution (diameter, 7 nm) were also plotted. Those of computer simulations (diameter, 50, 100, 200, 250, and 500 nm) at $[Hb]_{in}$ = 35 g/dl are plotted as *open circles*. Both *graphs* show that computer simulations recreate well the tendencies of the experimental results; $k'_{on}{}^{(NO)}$ decreases considerably with increasing $[Hb]_{in}$ and diameter, and $k'_{on}{}^{(CO)}$ does not show such changes.

size dependence of $k'_{on}{}^{(NO)}$ and the independence of $k'_{on}{}^{(CO)}$ were also recreated well as shown in Fig. 3*B*. The larger particle showed a slower rate of NO binding but not CO binding. It should be noted that this simulation does not consider the extracellular diffusion barrier and lipid membrane permeability.

The one-dimensional concentration changes of free NO molecules and unbound free hemes in each unit in one HbV ($[Hb]_{in}$ = 1 and 35 g/dl) are obtained by simulations, and the results are converted to a two-dimensional scheme, as shown in Fig. 4. In the case of HbV at $[Hb]_{in}$ = 1 g/dl, both dissolved free NO and unbound free hemes are already homogeneously distributed at 5 ms, indicating that NO diffuses rapidly into HbV, and the reaction proceeds quite homogeneously. On the other hand, HbV at $[Hb]_{in}$ = 35 g/dl showed heterogeneous distribution. The concentration gradients of both NO and heme change from the interior surface to the core. Even after 100 ms, the distributions are heterogeneous.

To clarify the influence of D_{NO} that changes with $[Hb]_{in}$ (Table 2), D_{NO} was fixed to the value in the bulk solution (2210 $\mu m^2\ s^{-1}$) to all HbV with different $[Hb]_{in}$. As shown in Fig. 5, the difference in $k'_{on}{}^{(NO)}$ is minimized considerably in comparison with the condition of variable D_{NO} at each $[Hb]_{in}$. This indicates that the lowered D_{NO} in the highly concentrated viscous Hb solution contributes considerably to the retardation of NO binding.

Extrapolation to Larger Particles (1000–8000 nm)—Computer simulations were performed to larger particles (diameter, 1000, 2000, and 8000 nm) in addition to smaller particles (≤500 nm); their apparent binding rate constants, $k'_{on}{}^{(NO)}$ and $k'_{on}{}^{(CO)}$, are plotted against the diameter to clarify the influence of diameters of particles encapsulating the 1 and 35 g/dl Hb solutions (Fig. 6). The experimental values of the Hb solution and HbV are also plotted; they show good coincidence. At $[Hb]_{in}$ = 35 g/dl, both NO binding and CO binding are remarkably retarded with larger diameters. Interestingly, there were threshold diameters for retardation of both NO and CO bindings, around 100 nm for $k'_{on}{}^{(NO)}$ and 1000 nm for $k'_{on}{}^{(CO)}$. Although HbV with smaller diameters shows almost identical $k'_{on}{}^{(CO)}$, the results of our computer simulation suggest that particles larger than 1000 nm would show retardation of CO binding in much the same manner as that with NO binding. At $[Hb]_{in}$ = 1 g/dl, both NO binding and CO binding showed less change in the binding rate constants that coincide the experimental results; however, the simulation predicts that the retardation becomes obvious with particles larger than ~1000 nm for NO binding, and

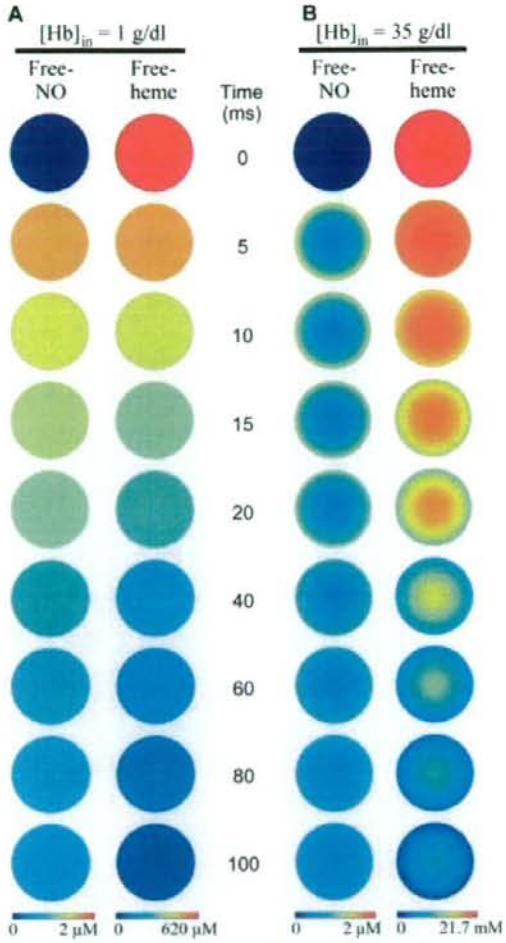

FIGURE 4. **Schematic two-dimensional representation of the simulated time courses of distributions of unbound free NO and unbound free heme in one HbV (250 nm).** *A*, at $[Hb]_{in}$ = 1 g/dl, both free NO and unbound hemes are distributed homogeneously at 5 ms, indicating that NO diffuses rapidly into HbV; the reaction proceeds homogeneously. *B*, at $[Hb]_{in}$ = 35 g/dl, both free NO and unbound hemes are distributed heterogeneously at any time. The concentration changes gradually from the surface to the core, indicating formation of the intracellular diffusion barrier. Particle diameter is fixed at 250 nm. It is easily speculated from the results that such gradients will be enhanced in larger particles.

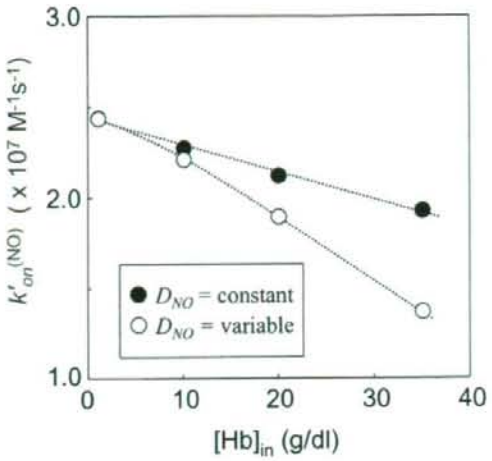

FIGURE 5. **Influence of D_{NO} on the retardation of NO binding to HbV.** Computer simulations of NO binding to HbV were performed under the assumption that the diffusion constant of NO (D_{NO}) is independent of $[Hb]_{in}$ (*closed circles*). D_{NO} was fixed to the value in the bulk solution (2210 $\mu m^2 s^{-1}$) to all HbV with different $[Hb]_{in}$. The HbV with a higher $[Hb]_{in}$ showed a slower rate of binding. However, the slope becomes gentle in comparison with the results of variable D_{NO} at each $[Hb]_{in}$ as shown in Table 2 (*open circles*). This indicates the contribution of the reduced D_{NO} in a highly viscous Hb solution to the retardation of NO binding. Particle diameter is fixed at 250 nm.

~2000 nm for CO binding. We can estimate the apparent binding rate constant of a particle encapsulating a 35-g/dl Hb solution with 8000-nm diameter, and $k'_{on}^{(NO)}$ and $k'_{on}^{(CO)}$ will be reduced to 5.6×10^5 and 7.3×10^4 $M^{-1} s^{-1}$, respectively. Overall, encapsulation of a 35-g/dl Hb solution in an 8000-nm particle would retard the NO binding by 2 orders and the CO binding by 1 order in comparison with the corresponding elementary reactions of the cell-free Hb solution.

DISCUSSION

Our primary finding is that NO binding of Hb is considerably retarded when a concentrated Hb solution is encapsulated in phospholipid vesicles (liposomes). On the other hand, CO binding of Hb shows no such retardation by encapsulation with particle size smaller than 500 nm. The phospholipid bilayer membrane itself has no barrier function to the gas diffusion, because the apparent binding rate constants of both NO and CO at $[Hb]_{in}$ = 1 g/dl and those of an acellular Hb solution were almost identical. In this study, using computer simulations, we propose that the determinant factor of retardation should be the intracellular, not extracellular, gas diffusion barrier in the case of HbV, which was induced by (i) the considerably large binding rate constant of NO to a heme of an Hb molecule, (ii) the numerous hemes as sites of gas entrapment at a high $[Hb]_{in}$, (iii) the slowed gas diffusion in the intracellular viscous Hb solution, and (iv) the longer diffusion distance in the larger particle diameter of the capsule (Fig. 7).

We reported the retardation of NO binding by Hb encapsulation in 1996 (30), which was earlier than the 1998 report of Liu *et al.* (6), who first showed that NO binding of Hb is retarded by the RBC cellular membrane. Rudolph *et al.* (26) attempted stopped-flow spectrophotometry of liposome-encapsulated Hb in 1997, expecting the retardation of the NO reaction by Hb encapsulation, but they identified no effect that was likely to have been attributable to the low $[Hb]_{in}$ (<14 g/dl) of their liposome-encapsulated Hb. In the present study, we intended more detailed analyses to clarify the mechanism of retardation, because it seems to have remained controversial in the last decade (20). It seems to us that these controversies are attributable to the complex and fragile structure of RBC and chemically unstable NO, which make it difficult to analyze the NO binding of RBC without causing hemolysis (2, 50). So-called competition experiments have been conducted between free Hb and RBC at a high hematocrit that would be a physiologically more

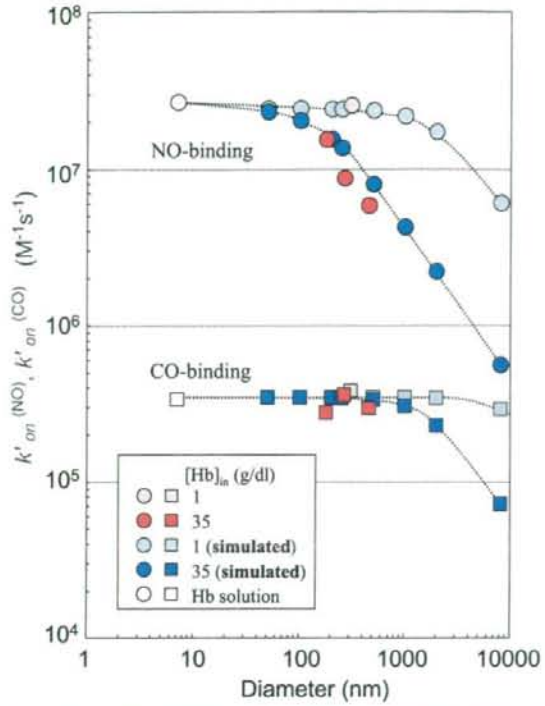

FIGURE 6. **Computer simulations of NO binding and CO binding by particles with different particle diameter.** At $[Hb]_{in}$ = 35 g/dl, the apparent CO binding rate constant, $k'_{on}{}^{(CO)}$, is almost identical up to 1000 nm in diameter; then it is reduced considerably, concomitant with increasing the diameter (*blue squares* in the *bottom*). On the other hand, $k'_{on}{}^{(NO)}$ decreases slightly up to 100 nm diameter; it then decreases steeply with enlarging particle diameter (*blue circles* in the *top*). In the case of $[Hb]_{in}$ = 1 g/dl, both NO binding (*light blue circles*) and CO binding (light blue squares) showed less change in the binding rate constants. However, the retardation becomes obvious when the particle diameter is larger than ~1000 nm for NO binding and even for CO binding when the diameter is larger than ~2000 nm. Experimental values for the Hb solution (*white circle* and *square*) and HbV (*pink* or *red squares* and *circles*) are close to the simulated values. The apparent binding rate constants, $k'_{on}{}^{(NO)}$ and $k'_{on}{}^{(CO)}$, of a spherical particle with diameter of 8000 nm and $[Hb]_{in}$ = 35 g/dl are estimated to be reduced to 5.6×10^5 and 7.3×10^4 M^{-1} s^{-1}, respectively. The reported $k'_{on}{}^{(NO)}$ values of a series of chemically modified HBOCs (diameter, 6–28 nm), about 3.0×10^7 M^{-1} s^{-1}, were identical to that of an unmodified Hb solution (38), which coincided well with our simulation.

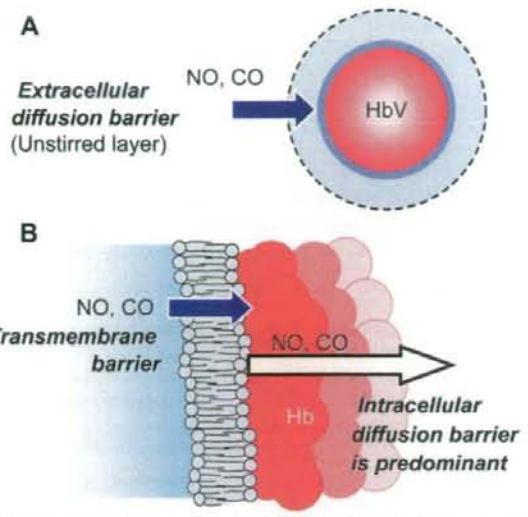

FIGURE 7. **Proposed mechanisms of retardation of gas binding by encapsulated Hbs.** *A*, it has been suggested that an unstirred layer near the outer surface of a cell would become an extracellular diffusion barrier to retard ligand bindings. However, our experimental results and computer simulations suggest that this is not a major process for retardation of ligand bindings in the case of HbV. *B*, the phospholipid bilayer membrane cannot have any barrier function to gas diffusion, because the apparent binding rate constants of both NO and CO at $[Hb]_{in}$ = 1 g/dl were close to those of an acellular Hb solution, as shown in Fig. 3. We propose that the determinant factor of retardation should be the intracellular diffusion barrier in the case of HbV, which is induced by (i) an intrinsically larger binding rate constant of NO to a heme in an Hb molecule, (ii) numerous hemes as sites of gas entrapment at a higher $[Hb]_{in}$, (iii) a slowed gas diffusion in the intracellular viscous Hb solution, and (iv) a longer gas diffusion distance in a larger capsule.

relevant condition (7, 50). However, it remains unclear for us whether the heterogeneous condition of a concentrated RBC suspension in a more static condition would be appropriate for an accurate kinetic measurement. Resealed RBCs were prepared to reduce the submembrane cytoskeletal layer or to reduce $[Hb]_{in}$ (2, 23), but it remains unknown whether hemolysis was suppressed completely after the complicated procedure and whether the electrolyte concentrations were maintained that might influence the Hb allostery and the resulting ligand binding profiles. We surmised that utilization of HbV, an artificially prepared model of RBC, would enable a systematic analysis, because the physicochemical parameters of HbV are adjustable, such as high $[Hb]_{in}$ up to 35 g/dl and particle diameter in a narrow range of P_{50}. Moreover, the physical stability of HbV is unexpectedly sufficient for stopped-flow spectrophotometry. We intentionally selected a low NO concentration (1.9 μM) to monitor the whole reaction of NO binding. Precedent reports of stopped-flow spectrophotometry of RBC at a higher NO concentration presented the problem not only of hemolysis but also the rate of NO reaction. It is so fast that a substantial part of the process occurs during the dead time (1–2 ms). On the other hand, in our study, a pseudo-first-order reaction is not appropriate for NO binding, and we calculated $k'_{on}{}^{(NO)}$ from the initial phase of the reaction because of a low NO concentration compared with the heme concentration. In such a condition, some redox charge transfer reaction would occur between heme and NO at a lower NO concentration (51). Another limitation of our simulation is the wide size distribution of HbV prepared using the extrusion method. $[Hb]_{in}$ was the concentration of the fed Hb solution for encapsulation, and we did not directly measure $[Hb]_{in}$ after encapsulation. These would be reasons for the deviation of the experimental results and the simplified computer simulation. However, it should be noted that our computer simulations recreated the tendencies of the experimental results of the ligand binding profiles of HbV.

In the computer simulation, we did not include the extracellular diffusion barrier, because HbV (250 nm) is much smaller than RBC (8 μm), and the diffusion of HbV as a particle should be much faster than that of RBC according to the Stokes-Einstein equation. The extracellular fluid near the surface should be stirred by the rapid movement of HbV. It is expected that the

thickness of the unstirred layer as an extracellular diffusion barrier would be much less for small HbV than that for RBC (1–3 μm) (2). Actually, results of the present computer simulations of HbV without consideration of the extracellular diffusion barrier clarified that the intracellular diffusion resistance is sufficient to explain the retardation of NO binding in the results of stopped-flow spectrophotometry, and possibly, our findings might suggest that the extracellular diffusion barrier is negligible even for RBC. This supports the results of Vaughn *et al.* (7) that the extracellular diffusion resistance is negligible. However, our data do not directly support the presence of transmembrane diffusion limitation, because the HbV at $[Hb]_{in} = 1$ g/dl and the cell-free Hb solution showed nearly identical $k'_{on}{}^{(NO)}$; actually, the computer simulation did not require the consideration of the membrane barrier. Han *et al.* (23) proposed that a submembrane cytoskeletal barrier would induce the resistance to the NO binding to bovine RBC using the RBC ghost. This might be possible to some extent if the submembrane cytoskeleton were to contain densely layered heme proteins such as adsorbed Hbs that could be the sites of rapidly binding NO. However, we believe that the intracellular concentrated Hb solution (about 35 g/dl) near the cytoskeleton of RBC can be the predominant barrier to further NO diffusion into RBC. Liu *et al.* (19) described that "NO that enters into RBC is immediately scavenged by the concentrated intracellular Hb so that NO concentration inside the RBC is maintained very close to zero," although they did not pay attention to it as the intracellular diffusion barrier.

The binding rate constant of CO of cell-free Hb molecule ($k_{on}{}^{(CO)}$) is well known to be much smaller than those of NO and O_2 (52). The rate-limiting step for CO binding is the internal bond formation with the heme iron. In fact, based on the electron theory, CO enters the globin hundreds of times before it finally forms a bond with the iron atom. Consequently, the overall bimolecular rate constant is normally small (53). The experimental finding that CO binding shows negligible retardation, even after encapsulation in HbV, also supports our proposal that rapid NO binding causes the sink of NO at the interior surface region of HbV and retards further NO diffusion into the core of HbV in combination of the lowered D_{NO} in the highly concentrated viscous Hb solution (45–48). However, it is expected that HbV with a much larger diameter can contribute to retardation, even for CO binding, as clarified by our computer simulation. Coin and Olson (2) compared the bindings of O_2, CO, and ethyl isocyanate to Hb with their elementary reaction constants, k_{on}, of 3×10^6, 2.0×10^5, and $2.1 \times 10^4\ M^{-1}\ s^{-1}$, respectively (1:10 and 1:100 differences). Results of that study showed that the difference between k_{on} of Hb and k'_{on} of RBC decreases for a slower reaction. The difference becomes very small for the binding of ethyl isocyanate, which clearly supports our data; a faster reaction tends to induce a stronger intracellular diffusion barrier and retards the reaction in comparison with the cell-free Hb solution.

In blood circulation in the presence of O_2, NO is inactivated mainly by NO dioxygenation by O_2-bound HBOCs and RBC. According to Herold *et al.* (54), the rate constant of the elementary reaction, HbO_2 and NO, is $8.9 \times 10^7\ M^{-1}\ s^{-1}$, which is faster than that of deoxyHb ($2.6 \times 10^7\ M^{-1}\ s^{-1}$). We predict that the reaction with HbO_2 should be much faster to form an intracellular diffusion barrier than that with deoxyHb. Consequently, the contribution of Hb encapsulation to the retardation should be pronounced. This can support the results of Azarov *et al.* (50) and Huang *et al.* (21), which showed that "the membrane barrier function" becomes more effective in limiting NO uptake for oxygenated RBC than the deoxygenated RBC, although their proposing mechanism is different from ours.

Our computer simulation system would be an effective tool to predict the ligand binding profiles of HbV with different Hb concentration and different particle size and other imaginary parameters. This can roughly simulate the NO binding and CO binding profiles of a spherical particle with a diameter identical to that of the major axis of RBC. The values of $k'_{on}{}^{(NO)}$ and $k'_{on}{}^{(CO)}$ of a spherical particle encapsulating 35-g/dl Hb with a diameter of about 8 μm are estimated, respectively, as 5.6×10^5 and $7.3 \times 10^4\ M^{-1}\ s^{-1}$. Those values resemble the precedent values of human RBC measured using stopped-flow spectrophotometry without causing hemolysis (<5%): $k'_{on}{}^{(NO)}$, $1.2 \times 10^5\ M^{-1}\ s^{-1}$; $k'_{on}{}^{(CO)}$, $6.5 \times 10^4\ M^{-1}\ s^{-1}$ (55); and $k'_{on}{}^{(CO)}$, $6.0 \times 10^4\ M^{-1}\ s^{-1}$ (31). On the other hand, our simulated $k'_{on}{}^{(NO)}$ would be faster than the values of RBC; $5.2 \times 10^4\ M^{-1}\ s^{-1}$ (6) and $1.4 \times 10^4\ M^{-1}\ s^{-1}$ (50), which are contradictorily much smaller than the CO binding rate constants of the above, which might suggest the presence of other mechanisms, such as the unstirred layer as the extracellular diffusion barrier in the case of large RBCs that diffuse slowly at a high Hct in their experiments. Even so, the retardation seems to be mainly induced by the intracellular diffusion barrier, because $k'_{on}{}^{(NO)}$ is reduced by 2 orders of magnitude in comparison with a cell-free Hb. Alternatively, we might consider the biconcave disk structure of RBC. Different P_{50} values of HbV (13–16 torrs) in comparison with that of human RBC (28 torrs) might also influence the binding rates.

Interestingly, the presence of the threshold diameters for retardation of ligand bindings is apparent, as shown in Fig. 6. The threshold diameter for CO is larger than that for NO, indicating that the slower reaction of CO binding allows a longer distance of gas diffusion before induction of an intracellular diffusion barrier than it allows with the more rapid NO binding. The rate-determining steps are the elementary gas-binding reaction for particles smaller than the threshold diameter and the gas diffusion for larger particles. It should be noted that the retardation is predicted for the larger particles at $[Hb]_{in} = 1$ g/dl, although the threshold diameter is increased to 1000 nm for NO binding and 2000 nm for CO binding.

The retardation of NO binding by Hb encapsulation cannot fully explain the phenomenon that HbV with a diameter of ~250 nm does not induce vasoconstriction after intravenous injection (13), because $k'_{on}{}^{(NO)}$ of HbV is much larger than that of RBC (10^4 to $10^5\ M^{-1}\ s^{-1}$). Any HBOC is much smaller in size than RBC and is distributed homogeneously in the plasma layer (5). Therefore, an RBC-free zone at the blood/endothelium interface becomes an HBOC-dissolved zone and might be a sink of NO (56, 57). Rohlfs *et al.* (38) reported that the NO binding rate constants of a series of chemically modified HBOCs (diameter, 6–28 nm) (58), measured using the laser flash photolysis, were identical to that of an unmodified Hb

solution, about 3.0×10^7 M^{-1} s^{-1}, which coincided well with our simulation in Fig. 6; particles with a diameter of less than 50 nm are almost identical. They concluded straightforwardly that NO uptake was not related to vasoconstriction, because polyethylene glycol-modified Hb did not exceptionally induce vasoconstriction, and other mechanisms are actually suggested in relation to molecular recognition and oxygen affinity (11, 59). We speculate the presence of another threshold particle diameter to penetrate across the perforated endothelial cell layer to approach a space (such as the space of Disse near the sinusoidal endothelial layer in a hepatic microcirculation or the space between the endothelium and the smooth muscle) where CO or NO is produced as a vasorelaxation factor to bind to soluble guanylate cyclase, which catalyzes the conversion of guanosine triphosphate to cyclic guanosine monophosphate (13, 18, 60, 61). As summarized by Olson *et al.* (16), both the retardation of the NO reaction (reduced NO affinity) (62) and the larger particle diameter are inferred to be keys to suppress vasoconstriction and hypertension induced by HBOCs.

In summary, we suggest the significant contribution of the intracellular diffusion barrier and the absence of lipid membrane barrier for NO uptake in the case of HbV. We speculate that the same findings might apply to RBCs. Although some discrepancies exist between the experimental results and computer simulations, we are surprised that such a simple simulation system can be an effective tool to predict the ligand binding reaction of HbV and larger particles, although the system is based merely on physicochemical parameters: the gas diffusion constant and elementary reaction rate constants. Our data provide a new insight into the cellular structures of RBC and HbV as an artificial oxygen carrier. Our next step will be to apply this system to recreate the ligand binding profiles of a biconcave disk shaped or parachute-like RBC and HbV suspension flowing heterogeneously in microvessels and in an artificial gas-permeable narrow tube (5) to identify additional mechanisms of the absence of vasoconstriction.

Acknowledgments—We thank Prof. M. Intaglietta (University of California, San Diego) and Prof. M. Suematsu (Keio University) for discussion related to the mechanism of ligand binding.

REFERENCES

1. Hartridge, H., and Roughton, F. J. W. (1927) *J. Physiol.* **62,** 232–242
2. Coin, J. T., and Olson, J. S. (1979) *J. Biol. Chem.* **254,** 1178–1190
3. Vandegriff, K. D., and Olson, J. S. (1984) *J. Biol. Chem.* **259,** 12619–12627
4. Page, T. C., Light, W. R., McKay, C. B., and Hellums, J. D. (1998) *Microvasc. Res.* **55,** 54–66
5. Sakai, H., Suzuki, Y., Kinoshita, M., Takeoka, S., Maeda, N., and Tsuchdia, E. (2003) *Am. J. Physiol.* **285,** H2543–H2555
6. Liu, X., Miller, M. J., Joshi, M. S., Sadowska-Krowicka, H., Clark, D. A., and Lancaster, J. R., Jr. (1998) *J. Biol. Chem.* **273,** 18709–19713
7. Vaughn, M. W., Huang, K. T., Kuo, L., and Liao, J. C. (2000) *J. Biol. Chem.* **275,** 2342–2348
8. Minneci, P. C., Deans, K. J., Zhi, H., Yuen, P. S., Star, R. A., Banks, S. M., Schechter, A. N., Natanson, C., Gladwin, M. T., and Solomon, S. B. (2005) *J. Clin. Invest.* **115,** 3409–3417
9. Hess, J. R., MacDonald, V. W., and Brinkley, W. W. (1993) *J. Appl. Physiol.* **74,** 1769–1778
10. Sloan, E. P., Koenigsberg, M., Gens, D., Cipolle, M., Runge, J., Mallory, M. N., and Rodman, G., Jr. (1999) *J. Am. Med. Assoc.* **282,** 1857–1864
11. Gulati, A., Barve, A., and Sen, A. P. (1999) *J. Lab. Clin. Med.* **133,** 112–119
12. Rochon, G., Caron, A., Toussaint-Hacquard, M., Alayash, A. I., Gentils, M., Labrude, P., Stoltz, J. F., and Menu, P. (2004) *Hypertension* **43,** 1110–1115
13. Sakai, H., Hara, H., Yuasa, M., Tsai, A. G., Takeoka, S., Tsuchida, E., and Intaglietta, M. (2000) *Am. J. Physiol.* **279,** H908–H915
14. Nakai, K., Ohta, T., Sakuma, I., Akama, K., Kobayashi, Y., Tokuyama, S., Kitabatake, A., Nakazato, Y., Takahashi, T. A., and Sekiguchi, S. (1996) *J. Cardiovasc. Pharmacol.* **28,** 115–123
15. Bunn, H. F. (1995) *Transfus. Clin. Biol.* **2,** 433–439
16. Olson, J. S., Foley, E. W., Rogge, C., Tsai, A. L., Doyle, M. P., and Lemon, D. D. (2004) *Free Radic. Biol. Med.* **36,** 685–697
17. Suematsu, M., Goda, N., Sano, T., Kashiwagi, S., Egawa, T., Shinoda, Y., and Ishimura, Y. (1995) *J. Clin. Invest.* **96,** 2431–2437
18. Goda, N., Suzuki, K., Naito, M., Takeoka, S., Tsuchida, E., Ishimura, Y., Tamatani, T., and Suematsu, M. (1998) *J. Clin. Invest.* **101,** 604–612
19. Liu, X., Samouilov, A., Lancaster, J. R., Jr., and Zweier, J. L. (2002) *J. Biol. Chem.* **277,** 26194–26199
20. Kim-Shapiro, D. B., Schechter, A. N., and Gladwin, M. T. (2006) *Arterioscler. Thromb. Vasc. Biol.* **26,** 697–705
21. Huang, K. T., Huang, Z., and Kim-Shapiro, D. B. (2007) *Nitric Oxide* **16,** 209–216
22. Huang, K. T., Han, T. H., Hyduke, D. R., Vaughn, M. W., Van Herle, H., Hein, T. W., Zhang, C., Kuo, L., and Liao, J. C. (2001) *Proc. Natl. Acad. Sci. U. S. A.* **98,** 11771–11776
23. Han, T. H., Pelling, A., Jeon, T. J., Gimzewski, J. K., and Liao, J. C. (2005) *Biochim. Biophys. Acta* **1723,** 135–142
24. Sakai, H., Masada, Y., Horinouchi, H., Yamamoto, M., Ikeda, E., Takeoka, S., Kobayashi, K., and Tsuchida, E. (2004) *Crit. Care Med.* **32,** 539–545
25. Sakai, H., Horinouchi, H., Yamamoto, M., Ikeda, E., Takeoka, S., Takaori, M., Tsuchida, E., and Kobayashi, K. (2006) *Transfusion* **46,** 339–347
26. Rudolph, A. S., Sulpizio, A., Hieble, P., MacDonald, V., Chavez, M., and Feuerstein, G. (1997) *J. Appl. Physiol.* **82,** 1826–1835
27. Chang, T. M. (2006) *Artif. Cells Blood Substit. Biotechnol.* **34,** 551–566
28. Djordjevich, L., and Miller, I. F. (1982) *Exp. Hematol.* **8,** 584–592
29. Sakai, H., Tomiyama, K. I., Sou, K., Takeoka, S., and Tsuchida, E. (2000) *Bioconjugate Chem.* **11,** 425–432
30. Sakai, H., Hamada, K., Takeoka, S., Nishide, H., and Tsuchida, E. (1996) *Polymer Adv. Technol.* **7,** 639–644
31. Olson, J. S. (1981) *Methods Enzymol.* **76,** 631–651
32. Takeoka, S., Ohgushi, T., Terase, K., Ohmori, T., and Tsuchida, E. (1996) *Langmuir* **12,** 1755–1759
33. Sakai, H., Tsai, A. G., Rohlfs, R. J., Hara, H., Takeoka, S., Tsuchida, E., and Intaglietta, M. (1999) *Am. J. Physiol.* **276,** H553–H562
34. Takeoka, S., Terase, K., Yokohama, H., Sakai, H., Nishide, H., and Tsuchida, E. (1994) *J. Macromol. Sci. Pure Appl. Chem., Part A* **31,** 97–108
35. Wang, L., Morizawa, K., Tokuyama, S., Satoh, T., and Tsuchida, E. (1992) *Polymer Adv. Technol.* **4,** 8–11
36. Sakai, H., Takeoka, S., Yokohama, H., Seino, Y., Nishide, H., and Tsuchida, E. (1993) *Protein Expression Purif.* **4,** 563–569
37. Sakai, H., Masada, Y., Takeoka, S., and Tsuchida, E. (2002) *J. Biochem. (Tokyo)* **131,** 611–617
38. Rohlfs, R. J., Bruner, E., Chiu, A., Gonzales, A., Gonzales, M. L., Magde, D., Magde, M. D. Jr., Vandegriff, K. D., and Winslow, R. M. (1998) *J. Biol. Chem.* **273,** 12128–12134
39. Szebeni, J., Breuer, J. H., Szelenyi, J. G., Bathori, G., Lelkes, G., and Hollan, S. R. (1984) *Biochim. Biophys. Acta* **798,** 60–67
40. Szebeni, J., Di Iorio, E. E., Hauser, H., and Winterhalter, K. H. (1985) *Biochemistry* **24,** 2827–2832
41. Baker, P. R., Lin, Y., Schopfer, F. J., Woodcock, S. R., Groeger, A. L., Batthyany, C., Sweeney, S., Long, M. H., Iles, K. E., Baker, L. M., Branchaud, B. P., Chen, Y. E., and Freeman, B. A. (2005) *J. Biol. Chem.* **280,** 42464–42475
42. Yokohama, H., Seino, Y., Chung, J., Sakai, H., Takeoka, S., Nishide, H., and Tsuchida, E. (1994) *Artif. Organs Today* **4,** 107–116
43. Sou, K., Naito, Y., Endo, T., Takeoka, S., and Tsuchida, E. (2003) *Biotechnol. Prog.* **19,** 1547–1552
44. Sakai, H., Hamada, K., Takeoka, S., Nishide, H., and Tsuchida, E. (1996) *Biotechnol. Prog.* **12,** 119–125
45. Nishide, H., Chen, X., and Tsuchida, E. (1997) *Artif. Cells Blood Substit.*

Immobil. Biotechnol. **25,** 335–346
46. Chen, X., Nishide, H., and Tsuchida, E. (1996) *Bull Chem. Soc. Jpn.* **69,** 255–259
47. Bouwer, S. T., Hoofd, L., and Kreuzer, F. (1997) *Biochim. Biophys. Acta* **1338,** 127–136
48. Minton, A. P., and Ross, P. D. (1978) *J. Phys. Chem.* **82,** 1934–1938
49. Sakai, H., Tomiyama, K., Masada, Y., Takeoka, S., Horinouchi, H., Kobayashi, K., and Tsuchida, E. (2003) *Clin. Chem. Lab. Med.* **41,** 222–231
50. Azarov, I., Huang, K. T., Basu, S., Gladwin, M. T., Hogg, N., and Kim-Shapiro, D. B. (2005) *J. Biol. Chem.* **280,** 39024–39032
51. Gow, A. J., and Stamler, J. S. (1998) *Nature* **391,** 169–173
52. Rose, E. J., and Hoffman, B. M. (1983) *J. Am. Chem. Soc.* **105,** 2866–2873
53. Olson, J. S., Foley, E. W., Maillett, D. H., and Paster, E. V. (2003) *Methods Mol. Med.* **82,** 65–91
54. Herold, S., Exner, M., and Nauser, T. (2001) *Biochemistry* **40,** 3385–3395
55. Carlsen, E., and Comroe, J. H. (1958) *J. Gen. Physiol.* **42,** 83–107
56. Kavdia, M., Tsoukias, N. M., and Popel, A. S. (2002) *Am. J. Physiol.* **282,** H2245–H2253
57. Ieffers, A., Gladwin, M. T., and Kim-Shapiro, D. B. (2006) *Free Radic. Biol. Med.* **41,** 1557–1565
58. Vandegriff, K. D., McCarthy, M., Rohlfs, R. J., and Winslow, R. M. (1997) *Biophys. Chem.* **69,** 23–30
59. Tsai, A. G., Cabrales, P., Manjula, B. N., Acharya, S. A., Winslow, R. M., and Intaglietta, M. (2006) *Blood* **108,** 3603–3610
60. Nakai, K., Sakuma, I., Ohta, T., Ando, J., Kitabatake, A., Nakazato, Y., and Takahashi, T. A. (1998) *J. Lab. Clin. Med.* **132,** 313–319
61. Matheson, B., Kwansa, H. E., Bucci, E., Rebel, A., and Koehler, R. C. (2002) *J. Appl. Physiol.* **93,** 1479–1486
62. Doherty, D. H., Doyle, M. P., Curry, S. R., Vali, R. J., Fattor, T. J., Olson, J. S., and Lemon, D. D. (1998) *Nat. Biotechnol.* **16,** 672–676

meso-Tetrakis(α,α,α,α-*o*-amidophenyl)porphinatoiron(II) Bearing a Proximal Histidyl Group at the β-Pyrrolic Position via an Acyl Bond: Synthesis and O_2 Coordination in Aqueous Media

Akito Nakagawa,[1] Teruyuki Komatsu,*[1,2] and Eishun Tsuchida*[1]
[1]*Advanced Research Institute for Science and Engineering, Waseda University, 3-4-1 Okubo, Shinjuku-ku, Tokyo 169-8555*
[2]*PRESTO, Japan Science and Technology Agency (JST)*

(Received February 16, 2007; CL-070182; E-mail: teruyuki@waseda.jp, eishun@waseda.jp)

meso-Tetrakis(α,α,α,α-*o*-(1-methylcyclohexanamido)phenyl)porphinatoiron(III) bearing a proximal histidyl group at the β-pyrrolic position via an acyl bond (**4c**) has been synthesized. Human serum albumin (HSA) incorporating the ferrous complex (**4d**) formed a stable O_2 adduct under physiological conditions (pH 7.4, 37 °C). Although an electron-withdrawing acyl group is attached to the porphyrin periphery, the O_2-binding affinity of HSA-**4d** was slightly higher than that of a similar analogue with a histidyl–alkylene group (**2d**).

In the active centers of hemoproteins, a basic amino acid residue, axially coordinated to the prosthetic heme group, namely the proximal base, plays a crucial role in controlling their biological functions, for example, histidine in hemoglobin (Hb) and cysteine in cytochrome P450. To mimic the versatile performances of the hemoproteins, numerous porphyrin derivatives have been synthesized over the past decades.[1,2] The most important factor in the molecular design of these compounds is how to confer the proximal base into the porphyrin structure by a covalent bond.

We successfully introduced a histidyl–alkylene group to the β-pyrrolic position of *meso*-tetrakis(α,α,α,α-*o*-(1-methylcyclohexanamido)phenyl)porphine (**1a**) using the Vilsmeier reaction.[3] Human serum albumin (HSA) incorporating the ferrous complex (**2d**) can reversibly bind and release O_2 under physiological conditions (pH 7.4, 37 °C) in a fashion similar to Hb and myoglobin.[3b] The advantage of this strategy is to confer the proximal histidine to the porphyrin periphery in the last step of the synthesis.[3,4] However, the preparation processes are still labor-intensive: (1) formylation of the porphyrin, followed by (2) demetallation of copper, (3) reduction of –CHO to $–CH_2OH$, (4) connection with glutaric acid, and (5) binding of terminal histidine.[3,4] If the axial base can be introduced into the superstructured porphyrin in a few steps, it will lead to creating a new field in the hemoprotein model chemistry.

In this communication, we report for the first time, the one-step introduction of the 4-carboxybutanoyl group into the β-pyrrolic position of *meso*-tetrakis(α,α,α,α-*o*-(1-methylcyclohexanamido)phenyl)porphyrin, which is easily converted into the hisitidine-linked porphyrin (**4a**) by other two processes. The O_2-binding property of the HSA hybrid incorporating the ferrous complex (**4d**) was then investigated in aqueous media.

The copper(II) complex of the parent porphyrin (**1b**) was synthesized according to our previously reported procedure.[3] We have found that the 4-carboxybutanoyl group is introduced by the Friedel–Crafts reaction using glutaric anhydride and aluminium chloride ($AlCl_3$) (Scheme 1). The progress of the reaction was monitored by the red shift of the absorption maxima

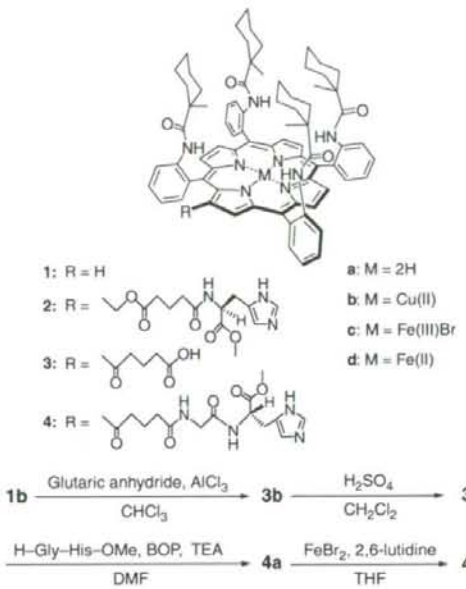

Scheme 1. Synthesis route of **4c**.

of the porphyrin and change in the R_f value during TLC. The brownish-red colored **3b** was purified by column chromatography and demetallated by H_2SO_4. The glycyl-*O*-methyl-L-histidine[5] was then coupled using benzotriazol-1-yl-oxytris(dimethylamino)phosphonium hexafluorophosphate (BOP). Finally, an iron insertion was carried out using $FeBr_2$ and 2,6-lutidine in anhydrous THF. The analytical data of all compounds described here were satisfactorily obtained (see Supporting Information).[6] The bathochromic shifts (3–7 nm) observed in the UV–vis absorption spectrum of **4a** compared to **2a** were due to the electron-withdrawing acyl group at the β-pyrrolic position.[6]

The ferric porphyrin (**4c**) in toluene was converted into the ferrous complex (**4d**) by reduction in a heterogeneous two-phase system (toluene/aq. $Na_2S_2O_4$) under an argon atmosphere.[4] The UV–vis absorption spectrum of the orange solution showed the formation of a five-N-coordinate high-spin complex (λ_{max}: 440, 544, 564 nm).[3,4,7] Upon exposure to O_2 or CO, the spectral pattern immediately changed to those of the O_2 adduct complex (λ_{max}: 429, 551 nm) or carbonyl complex (λ_{max}: 429, 544 nm).

The aqueous solution of the HSA-**4d** hybrid [in phosphate-buffered saline (PBS) solution (pH 7.4), [HSA]/[**4d**] = 1/4

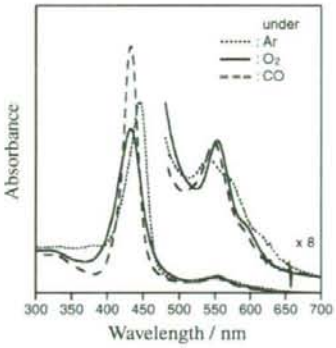

Figure 1. UV–vis absorption spectral changes of HSA-**4d** in PBS solution (pH 7.4) at 37 °C.

Table 1. O_2 binding parameters of HSA-porphinatoiron(II) in PBS solution (pH 7.4) at 25 °C[a]

Porphinatoiron(II)	$P_{1/2}$ /Torr	$k_{on}/\mu M^{-1} s^{-1}$		k_{off}/s^{-1}	
		fast	slow	fast	slow
2d[b]	1 (3)	54	8.8	89	14
4d	0.8 (2)	34	4.5	45	5.9

[a]The values in parenthesis are measured at 37 °C. [b]Ref 3b.

(mol/mol)] was prepared by a previously reported method.[3b] The UV–vis absorption spectrum of this aqueous solution under an argon atmosphere showed that **4d** formed a five-N-coordinate high-spin complex with an intramolecularly coordinated axial histidine (Figure 1). Upon exposure of HSA-**4d** to O_2, the absorption spectrum changed to that of the O_2 adduct complex. After reacting with the CO gas, a stable carbonyl complex was produced. The absorption maxima of HSA-**4d** showed 1–3 nm bathochromic shifts compared to those of the HSA-**2d** (Table S1).[3b,6]

The O_2-binding affinity of HSA-**4d** ($P_{1/2} = 0.8$ Torr) determined by the spectral changes at the different O_2 partial pressures was slightly higher than that of HSA-**2d** (Table 1). This is in significant contrast to the fact that the substitutions of two 3,8-vinyl groups of the imidazole-bound protoporphinatoiron(II) by acetyl groups decreased the O_2-binding affinity by 1/4–1/6 due to the reduction of the electron density in the porphyrin plane.[8,9] Our result suggested that (1) the reduced basicity of the porphyrin core by the introduction of one acyl group did not influence the O_2-binding equilibrium very much, and (2) that there is another structural factor that increases the O_2-binding affinity of the porphyrin.

To determine the association and dissociation rate constants for O_2 (k_{on}, k_{off}) to HSA-**4d**, the laser flash photolysis experiments were carried out.[3b,10,11] The absorption decay accompanying the O_2 recombination was composed of two phases of first-order kinetics, producing the fast and slow rebinding constants [k_{on}(fast) and k_{on}(slow)]. The k_{on}(fast) value was 7.6-fold higher than k_{on}(slow), and the molar concentration ratio of the two reactions was 3:1. The O_2 association to **4d** in the protein scaffold might be influenced by the microenvironment around the coordination site. This behavior was similarly observed in HSA-**2d**.[3b] The characteristics of the O_2 binding to **4d** was kinetically the low k_{off} values (approximately 1/2) compared to **2d**.

The structures of the ferrous complexes were then simulated.[12] It is remarkable that the porphyrin plane of **2d** in the five-coordinate high-spin complex was significantly domed compared to that of **4d** (Figure S1).[6] On the other hand, their O_2 adduct complexes showed similar structures having the flat porphyrin macrocycles. The difference in the five-coordinate species could be caused by the spacer moiety between the histidine and porphyrin. The rigid (histidyl-glycyl)carbonylbutanoyl group of **4d** presumably produces a favorable geometry to fix the proximal imidazole at the central iron(II) of the porphyrin, which could result in the relatively low dissociation rate constant of O_2.

In conclusion, we could successfully introduce the proximal histidyl group at the β-pyrrolic position of the *meso*-(tetrakis-*o*-amidophenyl)porphine via an acyl bond in two steps. The O_2 binding affinity was slightly higher than that of the imidazolyl–alkylene analogue, which might be due to the rigid structure of the spacer moiety between the histidine and porphyrin ring. This strategy would be useful to confer the proximal base to the superstructured porphyrin without any change in the activity, which allows us to create a new class of model heme compounds.

This work was supported by a Grant-in-Aid for Young Scientists (B) (No. 18750156) and for Scientific Research (No. 16350093) from JSPS, PRESTO from JST, and Health Science Research Grants from MHLW, Japan.

References and Notes

1 M. Momenteau, C. A. Reed, *Chem. Rev.* **1994**, *94*, 659, and references therein.
2 a) J. P. Collman, L. Fu, *Acc. Chem. Res.* **1999**, *32*, 455. b) J. P. Collman, R. Boulatov, C. J. Sunderland, *Chem. Rev.* **2004**, *104*, 561.
3 a) T. Komatsu, Y. Matsukawa, K. Miyatake, E. Tsuchida, *Chem. Lett.* **2001**, 668. b) T. Komatsu, Y. Matsukawa, E. Tsuchida, *Bioconjugate Chem.* **2002**, *13*, 397.
4 E. Tsuchida, T. Komatsu, S. Kumamoto, K. Ando, H. Nishide, *J. Chem. Soc., Perkin Trans. 2* **1995**, 747.
5 E. Monzani, L. Linati, L. Casella, L. D. Gioia, M. Favretto, M. Gullotti, F. Chillemi, *Inorg. Chem. Acta* **1998**, *273*, 339.
6 Supporting Information is available electronically on the CSJ-Journal Web site, http://www.csj.jp/journals/chem-lett/index.html.
7 J. P. Collman, J. I. Brauman, T. J. Collins, B. L. Iverson, G. Lang, R. B. Pettman, J. L. Sessler, M. A. Walters, *J. Am. Chem. Soc.* **1983**, *105*, 3038.
8 A. Nakagawa, N. Ohmichi, T. Komatsu, E. Tsuchida, *Org. Biomol. Chem.* **2004**, *2*, 3108.
9 T. G. Traylor, D. K. White, D. H. Campbell, A. P. Berzinis, *J. Am. Chem. Soc.* **1981**, *103*, 4932.
10 J. P. Collman, J. I. Brauman, B. L. Iverson, J. L. Sessler, R. M. Morris, Q. H. Gibson, *J. Am. Chem. Soc.* **1983**, *105*, 3052.
11 T. G. Traylor, S. Tsuchiya, D. Campbell, M. Mitchell, D. Stynes, N. Koga, *J. Am. Chem. Soc.* **1985**, *107*, 604.
12 The esff forcefield simulation was performed using an Insight II system (Molecular Simulation Inc.). The structure was generated by alternative minimizations and annealing dynamic calculations from 1000 to 100 K.

Published on the web (Advance View) April 14, 2007; doi:10.1246/cl.2007.640

Influence of O_2-carrying plasma hemoprotein "albumin-heme" on complement system and platelet activation *in vitro* and physiological responses to exchange transfusion

Teruyuki Komatsu,[1] Yubin Huang,[1] Shinobu Wakamoto,[2] Hideki Abe,[2] Mitsuhiro Fujihara,[2] Hiroshi Azuma,[2] Hisami Ikeda,[2] Hisashi Yamamoto,[3,4] Hirohisa Horinouchi,[3] Koichi Kobayashi,[3] Eishun Tsuchida[1]

[1]*Advanced Research Institute for Science and Engineering, Waseda University, 3-4-1 Okubo, Shinjuku-ku, Tokyo 169-8555, Japan*

[2]*Research Department, Hokkaido Red Cross Blood Center, 2-2 Yamanote, Nishi-ku, Sapporo 063-0002, Japan*

[3]*Department of General Thoracic Surgery, School of Medicine, Keio University, 35 Shinanomachi, Shinjuku-ku, Tokyo 160-8582, Japan*

[4]*Pharmaceutical Research Center, NIPRO Corp., 3023 Noji-cho, Kusatsu-shi, Shiga 525-0055, Japan*

Received 23 March 2006; revised 13 July 2006; accepted 25 July 2006
Published online 18 January 2007 in Wiley InterScience (www.interscience.wiley.com). DOI: 10.1002/jbm.a.31016

Abstract: Recombinant human serum albumin (HSA) including the synthetic iron(II)-porphyrin (FeP), albumin-heme (HSA-FeP), is a unique O_2-carrying plasma hemoprotein as a red blood cell substitute. We have investigated the possible influence of HSA-FeP on the complement system and platelet activation *in vitro*. The amounts of the serum complement titer CH_{50} and terminal complement complex SC5b-9 of human blood serum, incubated with HSA-FeP (10, 20, and 40 vol %), were almost the same as those of the corresponding samples with HSA. The effect of HSA-FeP on the platelet reactivity has been demonstrated by conformational changes in the membrane glycoprotein IIb/IIIa and surface expression of an α-granule membrane protein P-selectin. Platelet activation in response to the ADP-stimulation was not influenced by the presence of HSA-FeP. It can be concluded that the albumin-heme solution does not facilitate the immunological reaction and platelet activation. Moreover, a 20% exchange transfusion with HSA-FeP into anesthetized rats has been performed to evaluate the circulation and blood parameters for 6 h. Time course changes in all parameters showed features identical to the control group (without infusion) and HSA group. © 2007 Wiley Periodicals, Inc. J Biomed Mater Res 81A: 821–826, 2007

Key words: albumin-heme; complement system; exchange transfusion; platelet activation; RBC substitute

INTRODUCTION

There has been significant progress in red blood cell (RBC) substitutes in the past decade, and several hemoglobin (Hb)-based products are currently in clinical II/III trials.[1–4] We have also developed a unique albumin-based O_2-carrier "albumin-heme," which is composed of recombinant human serum albumin (HSA) including synthetic heme (2-[8-{*N*-(2-methylimidazolyl)}-octanoyloxymethyl]-5,10,15,20-tetrakis(α,α,α,α-*o*-pivalamido)phenylporphinatoiron(II)) (FeP, Scheme 1) (HSA-FeP).[5–7] The HSA-FeP solution has a high compatibility with the blood cell components, and its O_2-transporting capability was evaluated by animal experiments.[8,9] Nevertheless, animal studies cannot predict the potential effect on human responses. Especially, immunological reactions and platelet activity need not be the same as those in animals. In this study, we report the possible influence of HSA-FeP on the human complement system and platelet activation *in vitro*.

It is known that the complement cascade is activated in trauma patients with or without hemorrhagic shock.[10] The large volume administration of HSA-FeP as a blood alternative to the human body may affect the total serum complement activity. We have measured the amounts of complement titer CH_{50} and the terminal complement complex SC5b-9 of the human blood serum after incubation with HSA-FeP.

On the other hand, the platelet activation process involves an ordered sequence of events. In particular, the

Correspondence to: E. Tsuchida; e-mail: eishun@waseda.jp
Contract grant sponsor: Health Science Research Grants, MHLW, Japan

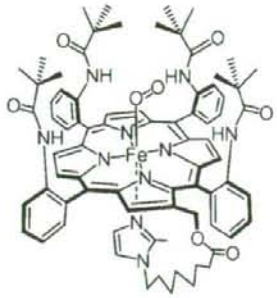

Scheme 1. Chemical structure of synthetic iron(II)-porphyrin (FeP) incorporated into HSA.

conformational changes in the membrane glycoprotein IIb/IIIa seem to be the most sensitive marker in the first event.[11–13] The activated GPIIb/IIIa creates a functional receptor for fibrinogen, which provides the link between adjacent platelets to form aggregates. The activation of this receptor can be detected by the specific monoclonal antibody PAC-1 that competes with fibrinogen.[11] The second event is the secretion of activation mediators, for example, ADP, serotonin, and thromboxane, resulting in further recruitment of platelets at the injured site.[14] The secretion process is accompanied by the rapid translocation of the α-granule membrane protein P-selectin (CD62P) to the outer membrane.[15,16] If the HSA-FeP solution activates the platelet, it may lead to amplifying the blood aggregation and inflammatory response. The PAC-1 binding and P-selectin surface expression have been assayed at the various levels of the ADP-stimulation.

Furthermore, we carried out the 20% exchange transfusion with the HSA-FeP solution into anesthetized rats and monitored the time courses of the circulation parameters (MAP, HR) and blood parameters (pH, PaO_2, PvO_2, $PaCO_2$) for 6 h.

MATERIALS AND METHODS

Materials

The recombinant human serum albumin (HSA, 25 wt %) was obtained from the NIPRO (Osaka). The HSA-FeP solution ([HSA]: 5.0 wt %, pH 7.4, [FeP]: 3.0 mM, COP: 21 mmHg, osmolarity: 300 mOsm, viscosity: 1.1 cP, endotoxin: <0.1 EU/mL, O_2-binding affinity ($P_{1/2}O_2$): 33 Torr) was prepared using our previously reported procedure.[8]

CH_{50} and SC5b-9

The human blood serum or plasma was well mixed with the HSA-FeP solution (the final concentration is 10, 20, and 40 vol %) and incubated for 1 h at 37°C. The CH_{50} value was determined by a 50% hemolysis assay based on Mayer's method with a commercial kit (New One point CH50 (KW), Japan BCG Supply, Tokyo). The SC5b-9 in the sample was determined using enzyme-linked immunosorbent assay kits (QUIDEL, Mountain View, CA).

PAC-1 and CD62P

The expression of PAC-1 and CD62P on platelets was measured as previously described.[17] Briefly, sodium citrate human whole blood was mixed with the HSA-FeP or HSA solution (the final concentration is 10, 20 and 40 vol %) and incubated for 10 min at 37°C. After adjusting the platelet concentration to

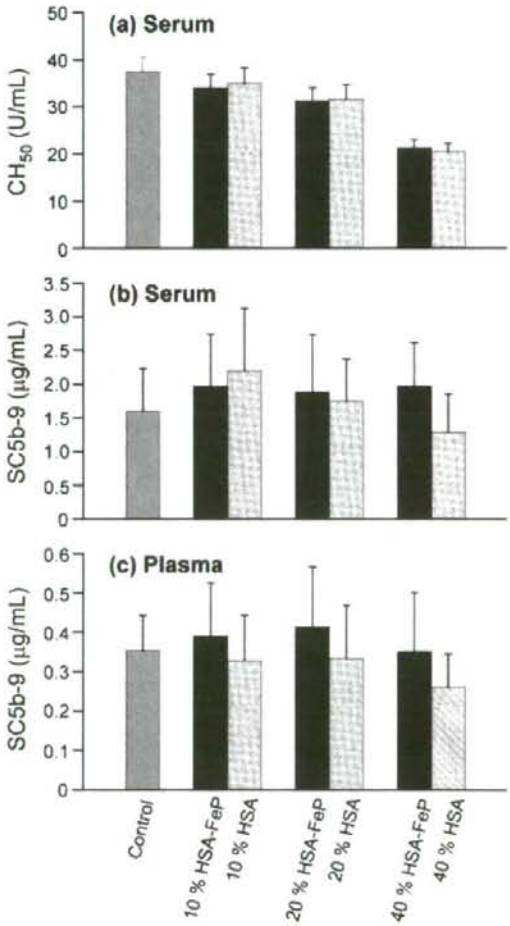

Figure 1. Influence of HSA-FeP on human serum complement after incubation for 1 h at 37°C; (a) serum complement titer (CH_{50}) in human blood serum, (b) terminal complement complex (SC5b-9) in human blood serum, and (c) SC5b-9 in human plasma. Each value represents the mean ± SD ($n = 5$).

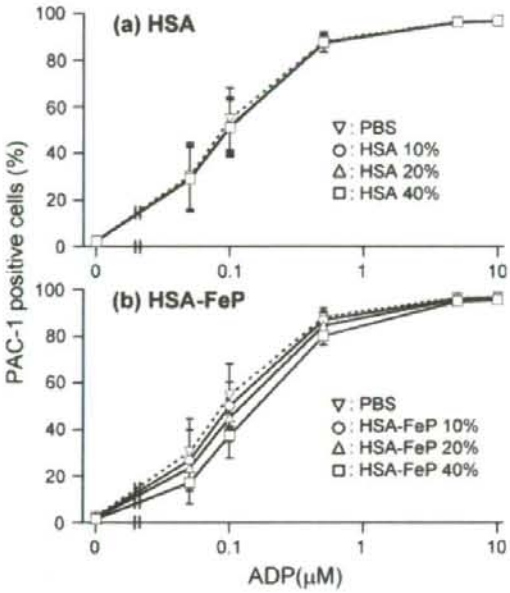

Figure 2. PAC-1 positive platelets in human whole blood mixed with (a) HSA-FeP and (b) HSA for 10 min at 37°C in response to various levels of ADP-stimulation. Each value represents the mean ± SD ($n = 5$).

4×10^5/20 μL by Hepes Tyrode's buffer (pH 7.3), a cocktail of FITC-conjugated PAC-1, PE-conjugated anti-CD62P, and PerCP-conjugated anti-CD42a was added in equal amounts. A certain amount of ADP was added (the final ADP concentration is 0.05, 0.1, 0.5, 5, and 10 μ*M*). The FITC-conjugated anti-mouse IgM, PE-conjugated anti-mouse IgG, and PerCP-conjugated anti-mouse IgG were used as the negative controls. All antibodies were purchased from BD Bioscience-Pharmingen (San Jose, CA). The mixture was reacted in the dark for 20 min at room temperature and fixed with 1% paraformaldehyde. The samples were analyzed by flow cytometry (LSR, BD, San Jose, CA). Fluorescence data from 10,000 platelet events were collected in the logarithmic mode. The platelet population was identified by the number of CD42a positive events. The increased activation of GPIIb/IIIa and expression of CD62P were demonstrated by the percent of PAC-1 and CD62P positive cells in the platelets, respectively.

All subjects enrolled in this research had responded to an Informed Consent which has been approved by The Committee on Human Research of Hokkaido Red Cross, and that this protocol was found acceptable by them.

Exchange transfusion

The animal experiments using Wistar rats (304 ± 7.2 g) were carried out according to our previously reported protocol.[9] After stabilization of the animal, the 20% exchange transfusion was performed by 1 mL blood withdrawal via the common carotid artery and 1 mL HSA-FeP infusion from the femoral vein (each 1 mL/min); a total of four repeating cycles ($n = 6$, HSA-FeP group). A blood sample was taken from the artery (0.3 mL) and vein (0.2 mL) at the following five times; (1) before, (2) immediately after, (3) 1 h after, (4) 3 h after, and (5) 6 h after the exchange transfusion. MAP, HR, O_2-pressure (PaO_2), CO_2-pressure ($PaCO_2$) and pH for the arterial blood, and the O_2-pressure (PvO_2) of the venous blood were measured. As a reference group, the 5 g/dL HSA solution was similarly administered to the rats ($n = 6$, HSA group).[9] Furthermore, six rats without infusion (operation only) were also used as a control group.[9]

All animal handlings were in accordance with the NIH guidelines for the care and use of laboratory animals. The protocol details were approved by the Animal Care and Use Committee of Keio University.

Data analysis

All data were represented by mean ± standard deviation (SD). Statistical analyses were performed by repeated analysis measures of variance (ANOVA) using a StatView (SAS Institute). Values of $p < 0.05$ were considered significant.

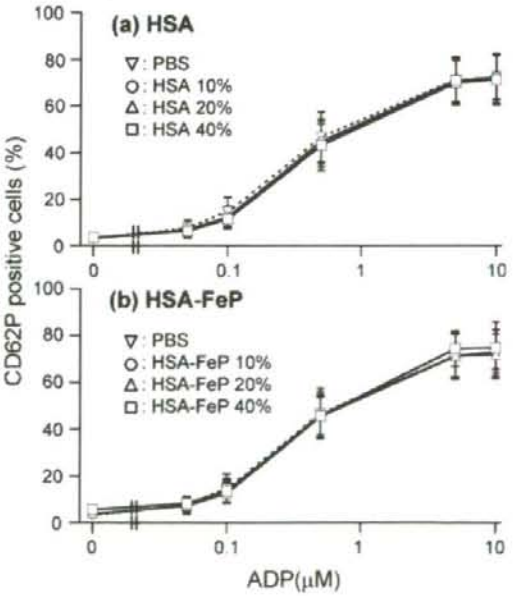

Figure 3. P-selectin expression on platelets in human whole blood mixed with (a) HSA-FeP and (b) HSA for 10 min at 37 C in response to various levels of ADP-stimulation. Each value represents the mean ± SD ($n = 5$).

RESULTS AND DISCUSSION

Complement system

Changes in the complement consumption are generally demonstrated by the complement titer CH_{50}. Ohtani et al. reported that the recombinant HSA, which is used for host albumin for HSA-FeP, shows the same immunochemical properties as the plasma HSA.[18] Thus the recombinant HSA should be a good reference in this experiment. The CH_{50} of the human blood serum incubated with 10, 20, and 40 vol % of the HSA-FeP solution were reasonably reduced in proportion to the each dilution ratio: 91, 83, and 57% of the control level [Fig. 1(a)]. The differences are almost the same as those observed in the HSA group, suggesting that the decrease in the CH_{50} with HSA-FeP did not involve any specific interaction.

On the other hand, the mean amounts of SC5b-9 in the human blood serum or plasma after the incubation with HSA-FeP were slightly higher than the control levels. However, all such differences were not significant within the experimental errors. Similar observations were found in the HSA group independent of the mixing ratio (10, 20, and 40 vol %). This implies that HSA-FeP does not enhance the production of SC5b-9.

Platelet activation

PAC-1 recognizes an epitope on the GPIIb/IIIa complex of activated platelets near the fibrinogen receptor.[19] We measured the percent of PAC-1 positive cells in the blood sample incubated with the HSA or HSA-FeP solution. When the ADP is absent, the fraction of the active cells was negligibly small, that is, 1.37–2.39%, independent of the mixing ratio of HSA or HSA-FeP (10, 20, and 40 vol %) (Fig. 2). The addition of a certain amount of ADP increased the PAC-1 positive cells, for instance, 96.9 % at 10 μM in the PBS group. It is rather remarkable that the coexistence of HSA and HSA-FeP (10–40 vol %) did not disturb this concentration dependence of the ADP-stimulation (Fig. 2).

The P-selectin (CD62P) on the activated platelet interacts with vascular endothelial cells to induce hemostasis. The percent of the P-selectin positive cells in the sample with HSA or HSA-FeP solution was 3.30–5.57% independent of the mixing ratio (10, 20, and 40 vol %) (Fig. 3). The addition of ADP enhances the numbers of active cells, and the concentration dependence curves observed in the HSA and HSA-FeP groups ([ADP] = 0.05–10 μM) were all identical to that of the PBS group. These results revealed that the platelet activation in response to the ADP-stimulation was not influenced by HSA-FeP. We concluded that albu-

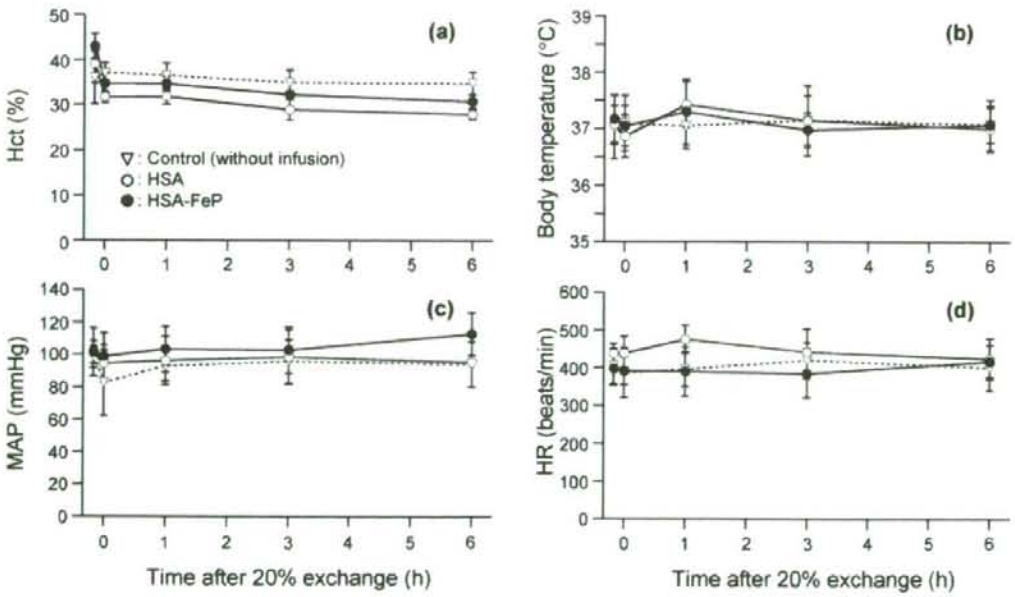

Figure 4. Time courses of (a) hematocrit (Hct), (b) body temperature, (c) mean arterial pressure (MAP), and (d) heart rate (HR) in anesthetized rats after 20% exchange transfusion with HSA-FeP or HSA solution. Each value represents the mean ± SD ($n = 6$).

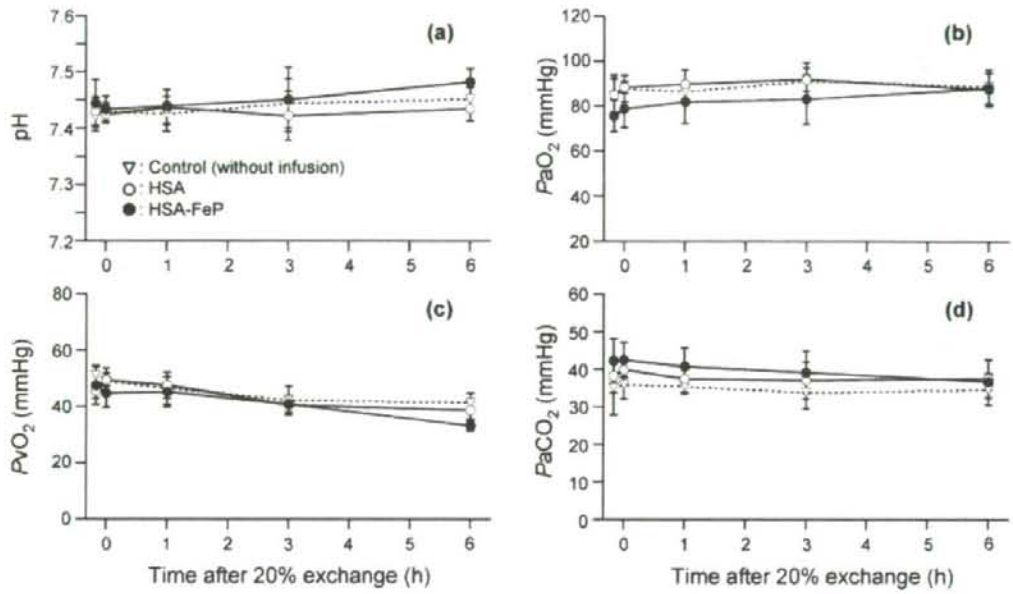

Figure 5. Time courses of (a) blood pH, (b) arterial blood O_2-pressure (PaO_2), (c) venous blood O_2-pressure (PvO_2), and (d) arterial blood CO_2-pressure ($PaCO_2$) in anesthetized rats after 20% exchange transfusion with HSA-FeP or HSA solution. Each value represents the mean ± SD ($n = 6$).

min-heme does not facilitate the immunological reaction and platelet activation in human blood at least based on the present test situation and degree.

Circulation parameters

After the 20% exchange transfusion with the HSA or HSA-FeP solution, Hct decreased ~80% of the basal values [Fig. 4(a)]. The body temperature of each group was maintained constant within 36.9–37.4°C during the experiments [Fig. 4(b)]. The time courses of MAP and HR of the HSA-FeP group were almost the same as those of the control or HSA group for 6 h [Fig. 4(c,d)]. Our previous studies showed that the infusion of HSA-FeP did not induce vasoconstriction and hypertension because of the low permeability of the albumin scaffold through the vascular endotheterlium.[20] It has been again demonstrated that absolutely no vasoactive response occurs after the 20% volume infusion of HSA-FeP.

Blood gas parameters

Changes in the blood gas parameters during the 20% exchange transfusion are shown in Figure 5(a–d). Differences in pH among the three groups were in the narrow range of 7.42–7.48 [Fig. 5(a)]. The PaO_2, PvO_2, and $PaCO_2$ values of the control, HSA, and HSA-FeP groups were also constant in the range of 78.9–91.8, 33.2–49.5, and 33.9–42.6 mmHg, respectively, by the end of the measurements [Fig. 5(b–d)]. These results revealed that HSA-FeP satisfies the initial preclinical safety as an RBC substitute.

In summary, one of the most prominent characteristics of the HSA-based O_2-carrier is its high blood compatibility, and no effect on the human immunological reaction and platelet activation. The appearance of the animals demonstrated no change for 6 h after the 20% exchange transfusion with HSA-FeP. The physiological responses in the HSA-FeP group were identical to those of the control and HSA groups. These results allow us to now undertake further advanced preclinical testing of this entirely synthetic O_2-carrier.

References

1. Chang TMS. Recent and future developments in modified hemoglobin and microencapsulated hemoglobin as red blood cell substitutes. Artif Cells Blood Substit Immobil Biotechnol 1997;25: 1–24.
2. Riess JG. Oxygen carriers ("blood substitute")—raison d'etre, chemistry, and some physiology. Chem Rev 2001;101:2797–2919.
3. Squires JE. Artificial blood. Science 2002;295:1002–1005.
4. Winslow R. Blood Substitutes. London: Elsevier; 2006.

5. Komatsu T, Hamamatsu K, Wu J, Tsuchida E. Physicochemical properties and O_2-coordination structure of human serum albumin incorporating tetrakis(*o*-pivamido)phenylporphyrinatoiron(II) derivatives. Bioconjug Chem 1999;10:82–86.
6. Tsuchida E, Komatsu T, Matsukawa Y, Hamamatsu K, Wu J. Human serum albumin incorporating tetrakis(*o*-pivalamido)-phenylporphinatoiron(II) derivative as a totally synthetic O_2-carrying hemoprotein. Bioconjug Chem 1999;10:797–802.
7. Komatsu T, Matsukawa Y, Tsuchida E. Effect of heme structure on O_2-binding properties of human serum albumin-heme hybrids: Intramolecular histidine coordination provides a stable O_2-adduct complex. Bioconjug Chem 2002;13:397–402.
8. Huang Y, Komatsu T, Nakagawa A, Tsuchida E, Kobayashi S. Compatibility in vitro of albumin-heme (O_2-carrier) with blood cell components. J Biomed Mater Res A 2003;66:292–297.
9. Hunag Y, Komatsu T, Yamamoto H, Horinouchi H, Kobayashi K, Tsuchida E. Exchange transfusion with entirely synthetic red-cell substitute albumin-heme into rats: Physiological responses and blood biochemical tests. J Biomed Mater Res A 2004;71:63–694.
10. Szebeni J, Wassef NM, Hartman KR, Alving CR. Complement activation in vitro by the red cell substitute, liposome-encapsulated hemoglobin: Mechanism of activation and inhibition by soluble complement receptor type 1. Transfusion 1997;37:150–159.
11. Shattil SJ, Hoxie A, Cunnington M, Brass LF. Changes in the platelet membrane glycoprotein IIb-IIIa complex during the platelet activation. J Biol Chem 1985;260:11107–11114.
12. Takagi J, Petre BM, Walz T, Springer TA. Global conformational rearrangements in integrin extracellular domains in outside-in and inside-out signaling. Cell 2002;110:599–611.
13. Xiao T, Takagi J, Coller BS, Wang JH, Springer TA. Structural basis for allostery in integrins and binding to fibrinogen-mimetic therapeutics. Nature 2004;432:59–67.
14. Marguerie GA, Plow EF, Edgington TS. Human platelets possess an inducible and saturable receptor specific for fibrinogen. J Biol Chem 1979;254:5357–5363.
15. Lasky LA. Selectin: Interpreters of cell-specific carbohydrate information during inflammation. Science 1992;258:964–969.
16. Stenberg PE, McEver RP, Shuman MA, Jacques YV, Bainton DF. A platelet alpha-granule membrane protein (GMP-140) is expressed on the plasma membrane after activation. J Cell Biol 1985;101:800–886.
17. Wakamoto S, Fujihara M, Abe H, Yamaguchi M, Azuma H, Ikeda H, Takeoka S, Tsuchida E. Effects of hemoglobin vesicles on resting and agonist-stimulated human platelets in vitro. Artif Cells Blood Substit Biotechnol 2005;33:101–111.
18. Ohtani W, Nawa Y, Takeshima K, Kamuro H, Kobayashi K, Ohmura T. Physiochemical and immunochemical properties of recombinant human serum albumin from *Pichia pastoris*. Anal Biochem 1998;256:56–62.
19. Taub R, Gould RJ, Garsky VM, Ciccarone TM, Hoxie J, Friedman PA, Shattil SJ. A monoclonal antibody against the platelet fibrinogen receptor contains a sequence that mimics a receptor recognition domain receptor. J Biol Chem 1989;264:259–265.
20. Tsuchida E, Komatsu T, Matsukawa Y, Nakagawa A, Sakai H, Kobayashi K, Suematsu M. Human serum albumin incorporating synthetic heme: Red blood cell substitute without hypertension by nitric oxide scavenging. J Biomed Mater Res A 2003;64:257–261.

Induced Long-Range Attractive Potentials of Human Serum Albumin by Ligand Binding

Takaaki Sato,[1,2,*] Teruyuki Komatsu,[2,3] Akito Nakagawa,[2] and Eishun Tsuchida[2,†]

[1]*Division of Pure and Applied Physics, Faculty of Science and Engineering, Waseda University, 3-4-1 Okubo, Shinjuku-ku, Tokyo 169-8555, Japan*

[2]*Advanced Research Institute for Science and Engineering, Waseda University, 3-4-1 Okubo, Shinjuku-ku, Tokyo 169-8555, Japan*

[3]*PRESTO, Japan Science and Technology Agency (JST), 4-1-8 Honcho, Kawaguchi-shi, Saitama 332-0012, Japan*

(Received 9 July 2006; published 15 May 2007)

Small-angle x-ray scattering and dielectric spectroscopy investigation on the solutions of recombinant human serum albumin and its heme hybrid revealed that heme incorporation induces a specific long-range attractive potential between protein molecules. This is evidenced by the enhanced forward intensity upon heme binding, despite no hindrance to rotatory Brownian motion, unbiased colloid osmotic pressure, and discontiguous nearest-neighbor distance, confirming monodispersity of the proteins. The heme-induced potential may play a trigger role in recognition of the ligand-filled human serum albumins in the circulatory system.

DOI: 10.1103/PhysRevLett.98.208101 PACS numbers: 87.14.Ee, 61.10.Eq, 83.80.Lz

Human serum albumin (HSA) is the most abundant plasma protein in our bloodstream, whose primary functions are transportation of hydrophobic molecules and adjustment of colloid osmotic pressure (COP) of blood [1]. Owing to its nonspecific ligand-binding capability, HSA has served many potential medical applications. Information on HSA-ligand interactions and their structural basis have recently been available by x-ray crystal structure analysis [2–5]. Such approaches have provided a structural foundation to create functional protein-ligand complexes. One of the promising materials is the rHSA-heme hybrid that can transport oxygen as hemoglobin does [6–9]. The material is currently investigated in preclinical tests as an artificial blood substitute [8]. Recent manifold interests in protein crystallography, critical phenomena, and disease processes have attracted increasing attention to interparticle interactions in globular protein solutions [10–15]. However, the fundamental problems like an influence of the ligand-binding upon protein-protein interactions remain elusive.

We investigated solutions of recombinant HSA (rHSA) (MW 66.5 kDa) and its heme hybrid [rHSA-heme; rHSA incorporating four iron-porphyrins (synthetic hemes)] [7]. Using small-angle x-ray scattering (SAXS), we scrutinized spatial correlations of these proteins in a 0.15M phosphate buffer saline (PBS) solution to fulfil ionic strength and pH close to physiological conditions and those in water to minimize ionic strength. The PBS solution of rHSA-heme (heme/rHSA = 4, mol/mol) was prepared according to our previously reported procedures [7]. The deionization of the protein sample was performed by several cycles of centrifugation/dilution with pure water using a Millipore Amicon Ultra to give aqueous solution of rHSA-heme. The solutions were passed through a 0.22 μm filter before all measurements. The deep red-colored, transparent solution of rHSA-heme can long be stored without precipitation or liquid-liquid phase separation. It has been confirmed that isoelectric point (pI), solution viscosity, and COP for rHSA-heme under the physiological environment are identical to those of rHSA.

All SAXS experiments were carried out by using a SAXSess camera (Anton Paar) in the q range of 0.072–5 nm^{-1}. A model-independent collimation-correction procedure was made via an indirect Fourier transformation (IFT) routine and/or based on a Lake algorithm. We also performed dielectric relaxation spectroscopy (DRS) experiments on aqueous rHSA and rHSA-heme solutions in the frequency range of $0.0005 \leq \nu/\mathrm{GHz} \leq 20$ using time domain reflectometry [16].

Figure 1 shows SAXS experiments on a concentration series of rHSA in PBS solution at 25 °C. The normalized scattered intensities $I(q)/c$, where $I(q)$ is the scattered intensity at scattering vector q and c the protein concentration, exhibit a decreasing forward intensity $I(q \to 0)/c$ with increasing c [Fig. 1(a)]. HSA carries a net negative charge of about 18 electronic charges at pH 7.4 [1]. Since the long-range electrostatic repulsion between rHSAs is efficiently screened in the PBS solutions, the suppressed forward intensity is mainly attributed to the decreased osmotic compressibility due to the increased particle number density. Lowering c results in the convergence of $I(q)/c$ to the intrinsic form factor $P(q)$ of rHSA, achieving the structure factor $S(q) \sim 1 (c \to 0)$.

The pair-distance distribution functions $p(r)$ of rHSA [Fig. 1(b)] in solution are obtained using generalized indirect Fourier transformation (GIFT) technique [17], for which we approximated $S(q)$ assuming a Yukawa potential and the Rogers-Young closure. The procedure confirms the existence of oblatelike particles having the maximum diameter of $D_{\max} \sim 8.0$–8.5 nm at all c. All features of $p(r)$ highly resemble those calculated from x-ray crystallography data on HSA (Protein Data Bank code 1UOR) [3].

Figure 2(a) presents variation of $I(q)$ of rHSA solutions, depending on the presence and absence of the heme incorporation and ionic strength of solvents. The more pronounced decrease of the forward intensity and the sig-

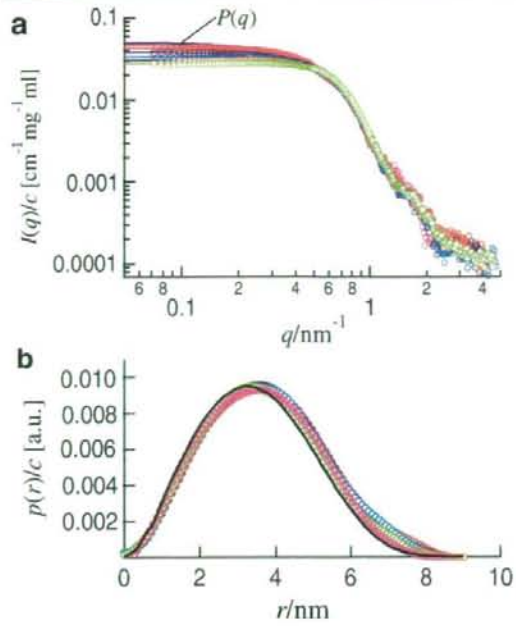

FIG. 1 (color online). (a) The normalized x-ray scattered intensities, $I(q)/c$, and (b) the pair-distance distribution functions, $p(r)$, of rHSA in 0.15M PBS solutions in $3.0 \leq c/\mathrm{mg\,ml^{-1}} \leq 50$. The black solid curve shown in (b) represents $p(r)$ calculated from the crystallography data on HSA [3].

nificant low-q shift of the monomer-monomer correlation peak position for aqueous rHSA reflect the only weakly screened, thus stronger electrostatic repulsions between the rHSA molecules. Importantly, we observed that heme-incorporated samples exhibit an enhanced forward intensity, which indicates that heme incorporation significantly enhances particle density fluctuations on a large length scale.

Further insights into the spatial correlations between the proteins are gained from the effective structure factors $S^{\mathrm{eff}}(q)$ [11] [Fig. 2(b)]. We extracted $S^{\mathrm{eff}}(q)$ by dividing $I(q)/c$ by $P(q)$ obtained from a dilute rHSA PBS solution. We confirmed that for rHSA-heme, lowering c from 10 to 3.5 mg ml^{-1}, leads to a significantly weaker relative low-q intensity, $I(q)/c$, as shown in Fig. 2. In terms of $S^{\mathrm{eff}}(q)$, rHSA under physiological condition still preserves the nature of a repulsively interacting charged colloid but behaves nearly as a hard sphere. If we apply a Yukawa potential model to $S^{\mathrm{eff}}(q)$ with *a priori* input of the solvent ionic strength, the effective protein charge of 18 ± 2 is obtained, being consistent with Ref. [1]. Solutions of rHSA-heme exhibit a similar low-q upturn in $S^{\mathrm{eff}}(q)$, independent of ionic strength. The observation suggests the emergence of a long-range attractive interaction [12,13] between the heme-incorporated rHSA molecules. However, this assignment is only valid when the monodispersity assumption of the protein is fulfilled. In the following, we carefully verify this interpretation, providing convincing evidence for monodispersity of rHSA-heme.

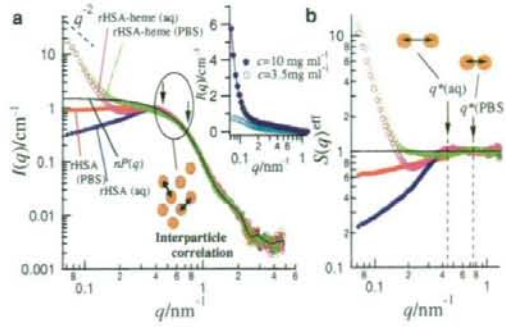

FIG. 2 (color online). (a) Variation of $I(q)$ and (b) the effective structure factors $S^{\mathrm{eff}}(q)$ for rHSA and rHSA-heme in aqueous and 0.15M PBS solutions of a fixed concentration $c = 30\ \mathrm{mg\,ml^{-1}}$. In the inset, the low-$q$ intensities for $c = 3.5\ \mathrm{mg\,ml^{-1}}$ and $c = 10\ \mathrm{mg\,ml^{-1}}$ are compared. Arrows on $S^{\mathrm{eff}}(q)$ highlight the monomer-monomer correlation peak positions q^*.

The peak in $S^{\mathrm{eff}}(q)$ arises from protein-protein positional correlations [Fig. 2(b)]. The mean nearest-neighbor distance d^* among the proteins is approximated as $\sim 2\pi/q^*$, where q^* is the scattering vector corresponding to the peak position of $S^{\mathrm{eff}}(q)$. Importantly, q^* is essentially independent before and after heme binding, but it simply depends on the solvent ionic strength related to the screening of the long-range electrostatic repulsion. In Fig. 3, we display a concentration series of $S^{\mathrm{eff}}(q)$ for rHSA and rHSA-heme solutions at different ionic strength. For aqueous rHSA and rHSA-heme, increasing c shifts q^* to higher values, holding a relation $q^* \propto n^{1/3}$ [Fig. 3(e)], where n is the particle number density. The finding clearly shows that both aqueous rHSA and rHSA-heme exhibit a typical feature of charged colloids at low ionic strength, maximizing d^*.

The identical COP (18 mmHg at $c = 50\ \mathrm{mg\,ml^{-1}}$) between the solutions of rHSA-heme and rHSA despite a half value for covalently dimerized rHSA at the same volume fraction [6] also rules out irreversible aggregate formation in rHSA-heme solutions. A simple model calculation demonstrates that a compact aggregate having several tens of aggregation number can never explain the observed low-q feature. No further enhancement of the low-q rise upon screening of the electrostatic repulsion excludes a strong short-range attraction as its origin.

Figure 4 presents complex dielectric spectra of rHSA and rHSA-heme solutions at various c. The relaxation time $\tau_{\mathrm{water}} \sim 8.3$ ps for the high-frequency process common for all solutions reflects the time scale of cooperative rearrangement of the hydrogen-bond network of bulk water [16,18,19]. Besides, the low-frequency relaxation, as-

signed to the rotational diffusion of the proteins [19,20], gives an excellent measure of dimer or higher aggregate formation. The identical relaxation times before and after heme binding, $\tau_{rHSA} \sim 52$–58 ns, provides identical effective molar volume for rHSA and rHSA-heme, $V^{eff} = 4.7 \times 10^4$ cm^3 mol^{-1} ($c \to 0$), according to the Stokes-Einstein-Debye equation, which is very close to the anticipated value of 4.9×10^4 cm^3 mol^{-1} from the molecular mass and specific volume of HSA. This reveals that the freedom of the rotational diffusive motion of the protein is not significantly affected by the heme incorporation.

We point out that in contrast to HSA, well-investigated aqueous lysozyme solutions [11–14,21,22] are already in aggregation regime; even at very low ionic strength, most of lysozyme molecules stick together due to its highly adhesive nature, which is demonstrated by the appearance of the low-q subpeak in $S^{eff}(q)$ and d^* coinciding with the diameter of the protein molecule. Although there arose a controversy as to whether the low-q rise for lysozyme solutions is due to a long-range attraction (LRA) [13,21] or large aggregate formation [22], as for rHSA-heme, the simultaneous observations of the low-q rise in $S^{eff}(q)$ with a host of evidence for monodispersity of the protein, such as d^* far exceeding the contact distance, no additional frictional force on the rotational diffusive motions, identical molecular volume with rHSA, and unbiased COP, provide a plausible argument for the emergence of a LRA. Note that any kind of protein aggregation requires the direct contact between the monomers. Generally, when the repulsion is so strong as to make the particles apart, the low-q rise can be explained only by a LRA [12].

The theoretical $S(q)$ analysis based on a two Yukawa potential model [13] has shown that the relatively longer attraction range than the repulsion one is necessary to produce the so-called zero-q peak in $S(q)$. The more pronounced low-q decrease in $S^{eff}(q)$ for aqueous rHSA is clearly taken over by the deeper dip in $S^{eff}(q)$ for aqueous rHSA-heme, which indicates that the electrostatic repulsion is still active in rHSA-heme solutions and the attraction range is greater than the range of the weakly screened electrostatic repulsion.

For further quantitative description, we tested a two Yukawa model [12,13] for $S^{eff}(q)$ of rHSA-heme. When the attraction range is very long, the model produces a downward convex low-q rise and a huge zero-q intensity reaching more than ~1000 even at small c. However, $S(q)$ starts to rise at $q \leq 0.1$ nm^{-1}, whereas we observed the onset around $q = 0.2$ nm^{-1}. The real expression for a LRA and its potential shape are still not very clear, but the formalism of the potential should significantly affect the low-q shape of $S(q)$. If the system exhibits more slowly decaying attractive potential than the Yukawa decay at small-r, the onset of the low-q rise is expected to shift to higher-q values than that predicted by the Yukawa LRA model.

It is important to recognize that isotropic interaction is not self-evident for any kind of protein system because proteins have irregular shape and inhomogeneously distributed patches by nature. However, until now, almost all experimental and theoretical works on the interactions proteins have been performed based on mean spherical approximation (MSA) and an isotropic interaction assumption [10–15,23]. The recent theoretical work of Bianchi *et al.* [24] revealed that particles interacting with an anisotropic attractive potential can enhance anomalous density fluctuations or gel-network formation even at very low volume fractions. This also implies that anisotropic potentials caused by a site-specific interaction or inhomogeneous distributions of charge or hydrophobic patches may generate unexpectedly drastic effects on the spatial correlations of proteins, where the inherent limitation of small-angle scattering technique lies in the fact that such anisotropic interactions are reduced into one-dimensional $S(q)$. Nevertheless, carefully confirmed monodispersity of rHSA-heme leads us to conclude that our present interpretation based on a LRA is still broadly correct, even if the actual situation is much more complicated, where anisotropic interactions may affect the spatial correlation of the proteins.

Compared to the well-developed short-range attraction and long-range electrostatic repulsion [11,13,23], the general understanding of a LRA of proteins in solution

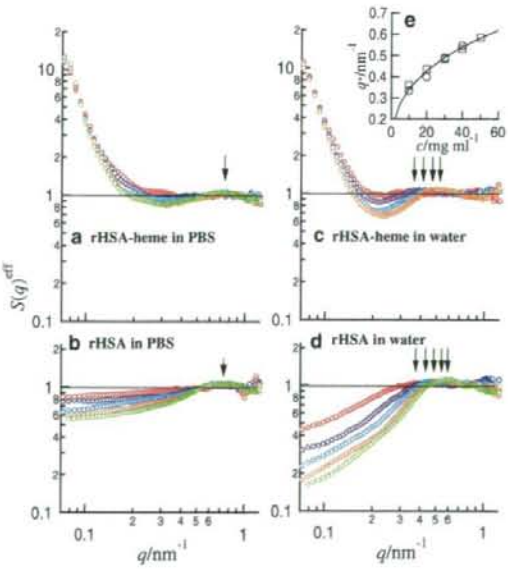

FIG. 3 (color online). Effects of concentration, ionic strength, and heme binding on $S^{eff}(q)$. (a) rHSA-heme and (b) rHSA in 0.15M PBS solutions and (c) rHSA-heme and (d) rHSA in aqueous solutions in $10 \leq c/\text{mg ml}^{-1} \leq 50$ (an increment of 10 mg ml^{-1}). (e) The protein-protein correlation peak position q^* in $S^{eff}(q)$ for aqueous rHSA (□) and rHSA-heme (○) as a function of c.

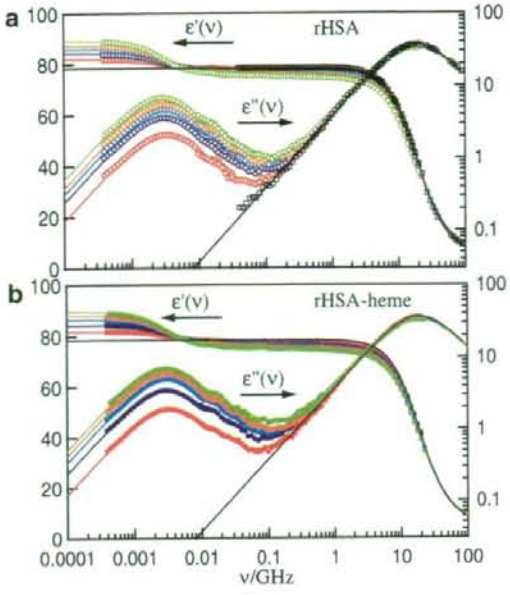

FIG. 4 (color online). Complex dielectric spectra of aqueous solutions of (a) rHSA and (b) rHSA-heme in $10 \leq c/\mathrm{mg\,ml^{-1}} \leq 50$ (an increment of 10 mg ml^{-1} from the bottom) at 25 °C.

[12,13,15] is at an incipient stage. Judging from unbiased $p\mathbf{I}(= 4.9)$ and polarization fluctuation amplitudes for rHSA-heme, net charges and their distributions are unlikely to be modified by heme binding, whereas how the occupation of the ligand-binding site allosterically affects the electrostatic interaction of the protein is unclear. The physical origin of a LRA might be entoropic driven, possibly due to modulated hydrophobic patches and their inhomogeneous distributions.

HSA binds heme; the rHSA-heme hybrid takes advantage of this naturally occurring process. In the human body, heme released from methemoglobin is immediately captured by hemopexin or HSA acting as scavengers, and it is efficiently transported to the liver for methabolism [25,26]. Since the emergence of the collective nature of HSAs while preserving the monodispersity could be an efficient way to give the ligand-filled HSA molecules a sort of marker, our data suggest that the heme-bound or -unbound HSAs may be recognized in the bloodstream in terms of the presence and absence of the LRA. Therefore, the optimization of the interparticle potential will be a key to the control of distribution, circulation persistence, and metabolism of functional ligands for medical applications.

This work was partly supported by MEXT, the Grant in Aid for Young Scientists (B) (No. 18740264), and by JSPS, the Grant in Aid for Scientific Research (B) (No. 16350093). T. S. acknowledges the 21st century COE program at Waseda University funded by MEXT. The authors appreciate the strong support of the late Professor Hironobu Kunieda for SAXS measurements and thank Professor Sow-Hsin Chen and Dr. Yun Liu for providing the MATLAB code for two Yukawa model [13].

*Email address: takaaki.sato@waseda.jp
†Email address: eishun@waseda.jp

[1] T. Peters, *All About Albumin: Biochemistry, Genetics, and Medical Applications* (Academic, New York, 1996).
[2] P. A. Zunszain *et al.*, BMC Struct. Biol. **3**, 6 (2003).
[3] X. M. He and D. C. Carter, Nature (London) **358**, 209 (1992).
[4] S. Curry *et al.*, Nat. Struct. Biol. **5**, 827 (1998).
[5] J. Ghuman *et al.*, J. Mol. Biol. **353**, 38 (2005).
[6] T. Komatsu *et al.*, Macromolecules **32**, 8388 (1999).
[7] T. Komatsu, Y. Matsukawa, and E. Tsuchida, Bioconjugate Chemistry **13**, 397 (2002).
[8] T. Komatsu *et al.*, J. Biomed. Mater. Res. **71A**, 644 (2004).
[9] T. Komatsu *et al.*, J. Am. Chem. Soc. **127**, 15 933 (2005).
[10] A. Tardieu *et al.*, J. Cryst. Growth **196**, 193 (1999).
[11] A. Stradner *et al.*, Nature (London) **432**, 492 (2004).
[12] Y. Liu *et al.*, Phys. Rev. Lett. **95**, 118102 (2005).
[13] Y. Liu, W. R. Chen, and S. H. Chen, J. Chem. Phys. **122**, 044507 (2005).
[14] M. Malfois, F. Bonnete, L. Belloni, and A. Tardieu, J. Chem. Phys. **105**, 3290 (1996).
[15] M. G. Noro, N. Kern, and D. Frenkel, Europhys. Lett. **48**, 332 (1999).
[16] T. Sato and R. Buchner, J. Phys. Chem. A **108**, 5007 (2004).
[17] G. Fritz, A. Bergmann, and O. Glatter, J. Chem. Phys. **113**, 9733 (2000).
[18] T. Fukasawa *et al.*, Phys. Rev. Lett. **95**, 197802 (2005).
[19] N. Nandi, K. Bhattacharyya, and B. Bagchi, Chem. Rev. **100**, 2013 (2000).
[20] Y. Hayashi *et al.*, Biophys. J. **79**, 1023 (2000).
[21] Y. Liu *et al.*, Phys. Rev. Lett. **96**, 219802 (2006).
[22] A. Stradner, F. Cardinaux, and P. Schurtenberger, Phys. Rev. Lett. **96**, 219801 (2006).
[23] F. Sciortino *et al.*, Phys. Rev. Lett. **93**, 055701 (2004).
[24] E. Bianchi *et al.*, Phys. Rev. Lett. **97**, 168301 (2006).
[25] V. Jeney, J. W. Eaton, and G. Balla *et al.*, Blood **100**, 879 (2002).
[26] E. Tolosano and F. Altruda, DNA and Cell Biology **21**, 297 (2002).

O_2-Binding Albumin Thin Films: Solid Membranes of Poly(ethylene glycol)-Conjugated Human Serum Albumin Incorporating Iron Porphyrin

Akito Nakagawa,[†] Teruyuki Komatsu,[†,‡,*] Yubin Huang,[†] Gang Lu,[†] and Eishun Tsuchida[†,*]

Research Institute for Science and Engineering, Waseda University, 3-4-1 Okubo, Shinjuku-ku, Tokyo 169-8555 Japan, and PRESTO, Japan Science and Technology Agency (JST), 4-1-8 Honcho, Kawaguchi-shi, Saitama 332-0012, Japan.
Received March 14, 2007; Revised Manuscript Received July 7, 2007

Poly(ethylene glycol) (PEG)-conjugated human serum albumin (HSA) incorporating the tetrakis(α,α,α,α-*o*-amidophenyl)porphinatoiron(II) derivative (FeP) [PEG(HSA−FeP)] is a unique plasma protein-based O_2 carrier as a red blood cell substitute. The aqueous solution of PEG(HSA−FeP) [mw of PEG: 2-kDa (PEG_2) or 5-kDa (PEG_5)] was evaporated on a glass surface to produce a red-colored solid membrane. Scanning electron microscopy observations revealed that the PEG_2(HSA−FeP) membrane consisted of two parts: (i) a surface layer made of a fibrous component (10 μm thickness), and (ii) a bottom layer of an amorphous phase (5 μm thickness). The condensed solution provided a thick membrane (70 μm), which also has the amorphous bottom layer. On the other hand, the PEG_5(HSA−FeP) produced homogeneous membrane made of the fibrous component. The FeP active sites in the solid membrane formed very stable O_2-adduct complexes at 37 °C with a half-lifetime of 40 h. The O_2-binding affinity of the PEG_2(HSA−FeP) membrane ($P_{1/2}$ = 40 Torr, 25 °C) was 4-fold lower than that in aqueous solution, which is kinetically due to the low association rate constant. The membrane was soluble again in water and organic solvents (ethanol and chloroform) without deformation of the secondary structure of the protein. The addition of hyaluronic acid gave a free-standing flexible thin film, and it can also bind and release O_2 as well. These O_2-carrying albumin membranes with a micrometer-thickness would be of significant medical importance for a variety of clinical treatments.

INTRODUCTION

Covalently surface-modified proteins with poly(ethylene glycol) (PEG) show a number of unique properties that make them of interest in a range of practical applications (*1*−*6*). The most beneficial effect of the PEG conjugation from a biological aspect is to confer a nonimmunogenicity to the proteins, rendering them invisible in the body (*7*−*10*). Several classes of protein drugs, such as enzymes and cytokines, have already been approved by the FDA (*4*, *5*), and one of the expected compounds is a PEG-conjugated hemoglobin (PEG-Hb) for use as artificial blood (*11*, *12*). The optimized product has completed a phase I trial and is currently undergoing a phase II safety study (*13*). Second, the PEG modification allows the proteins to be soluble in nonaqueous solvents (benzene, ethanol, and chloroform, etc.) (*14*−*16*). In organic solutions, the proteins exhibited new characteristics, for example, a high thermal stability and a different substrate selectivity. Third, the aqueous PEGylated proteins can be dried on a flat surface to produce solid membranes without any loss of their original activities. However, only limited characterization has been performed on the PEG-conjugated proteins in the solid state.

Recombinant human serum albumin (HSA) incorporating the tetrakis{α,α,α,α-*o*-(1-methylcyclohexanamido)phenyl}-porphinatoiron(II) derivative (FeP, Figure 1) (HSA−FeP) is a unique plasma protein-based O_2 carrier (*17*, *18*). This entirely synthetic hemoprotein can reversibly bind and release O_2 under physiological conditions (pH 7.4, 37 °C) in a fashion similar to Hb. It has also been demonstrated that the surface decoration of HSA−FeP by PEG improved its circulation persistence in the bloodstream (*19*). The PEG(HSA−FeP) is now the most promising material for an entirely synthetic red blood cell substitute.

We have recently found that the aqueous PEG(HSA−FeP) solution cast on the glass surface produces a very smooth solid membrane. The spectroscopic measurements revealed that a reversible O_2 binding to FeP took place in the red-colored membrane. We now report our new findings on the layered film structures of the PEG-conjugated artificial hemoprotein and their O_2-binding behavior.

EXPERIMENTAL PROCEDURES

Materials and Apparatus. All reagents were purchased from commercial sources as special grades and used without further purification. 2-{8-(2-Methylimidazolyl-1-yl)octanoyloxymethyl}-5,10,15,20-tetrakis{α,α,α,α-o-(1-methylcyclohexanamido)-phenyl}porphinatoiron(II) (FeP) was synthesized according to our previously reported procedures (*17*, *20*). Recombinant HSA was provided by the NIPRO Corp. (Osaka, Japan). 2-Iminothiolane hydrochloride (IMT) was purchased from Wako Pure Chemical Industries, Ltd. (Osaka, Japan). α-[3-(3-Maleimido-1-oxopropyl)amino]propyl-ω-methoxy PEG [averaged mw: 2333, Sunbright ME-020MA, PEG_2, and averaged mw: 5207, Sunbright MEMAL-50H, PEG_5) was purchased from the NOF Corp. (Tokyo, Japan). Hyaluronic acid sodium salt (HA, mw: 1.9−2.7 × 10^3 kDa) was a gift from Shiseido Co., Ltd. (Tokyo, Japan). The water was deionized using Millipore Elix and Simpli Lab-UV. The UV−vis absorption spectra were recorded using an Agilent 8453 UV−visible spectrophotometer fitted with an Agilent 89090A temperature control unit. The circular dichroism (CD) spectra were obtained using a JASCO J-820 spectropolarimeter over the range of 200−250 nm.

* Corresponding author. (E.T.) Tel: +81-3-5286-3120, fax: +81-3-3205-4740, e-mail: eishun@waseda.jp. (T.K.) E-mail: teruyuki@waseda.jp.
† Waseda University.
‡ Japan Science and Technology Agency.

10.1021/bc070086m CCC: $37.00
Published on Web 08/16/2007